Characterizing Phenotypic Differences between Two Clades of Influenza A Viruses from the 2016-17 and 2017-18 U.S. Flu Seasons

by

David Jacobs

A dissertation submitted to the Johns Hopkins University in conformity with the requirements for the degree of Master of Science.

Baltimore, Maryland

April 2019

Abstract

The severity of the influenza outbreak in the United States during the 2017-18 season surpassed that of the 2016-17 season, with a case load reminiscent of the H1N1 pandemic of 2009-10. This increase in severity occurred despite the fact that both seasons' H3N2 vaccine strain, derived from a clade 3C.2a virus, was from the same clade as the most commonly circulating viruses. Previous work conducted in the Pekosz laboratory determined that, between the 2016-17 and 2017-18 seasons, viruses of the 3C.2a1 clade reassorted with both 3C.2a2 and 3C.3a viruses. It was hypothesized that these reassortments might have contributed to the observed increase in virulence during the 2017-18 season. The results of these studies showed that 3C.3a viruses from both the 2016-17 and 2017-18 seasons, including the reassortant 3C.3a viruses, replicated to higher titers at earlier times post-infection in both immortalized cells and primary cell cultures than 3C.2a1 viruses. Additionally, 2017-18 3C.3a reassortant viruses produced larger plaques than either 2016-17 3C.2a1 or 3C.3a viruses. Taken together, these results suggest that 3C.3a reassortant viruses obtained a fitness advantage over the 3C.2a1 parental strain. To determine which gene segments were associated with this increased fitness, 3C.2a1 viruses with gene segments from the 2016-17 season and a single gene segment from the reassorted 3C.3a virus – either HA, M or NS – were clonally generated and examined for their replication phenotypes. An initial MDCK-Siat growth curve conducted with rescued monoreassortant 3C.2a1 viruses containing either 3C.3a HA, M or NS from the 2017-18 reassortant 3C.3a clade showed that the 3C.2a1 virus bearing the 3C.3a HA gene segment best recapitulated the phenotype of the 2017-18 3C.3a reassortant virus, suggesting that the HA gene segment is contributing substantially to the difference in the phenotype observed between the 3C.3a and 3C.2a1 clades.

Primary reader: Dr. Andrew Pekosz

Secondary reader: Dr. Sabra Klein

Acknowledgements

I would like to thank Dr. Andrew Pekosz for taking me into his laboratory and advising me on experimental directions throughout the research process. His dedication to my success was clear from my very first day in the lab, and I am in awe of his kindness and grateful for his insight. Dr. Hsuan Liu deserves special mention for bringing me up to speed on experimental protocols used routinely in the lab and answering many, many questions regarding their execution. Dr. Jason Westerbeck was instrumental in helping me master new techniques and quantify the data I was generating, as well as sharing his own data for comparison purposes. All members of the Pekosz lab were available to help troubleshoot difficult experiments and offer feedback, support, and sugary items to sustain me. Similarly, the Klein and Davis labs offered helpful insights into my work and provided camaraderie on a daily basis, and I must especially thank Dr. Sabra Klein for her help as the second reader of this thesis.

Beyond the lab, I of course want to thank my parents for supporting my dream of becoming a disease detective and giving me the ability to do so debt free. My ScM cohort members helped me become more social, and I appreciate their support throughout this process – right from the dreaded immunology courses through comps and in the final stretch of writing this very thesis. Special thanks and affection are reserved for Kip Strother and Gaby Madrigal, who perhaps more than anyone else are responsible for me actually graduating.

And, finally, a small dedication – Kurtis Johnson, a friend through Kip, passed away just prior to the completion of this thesis. Though I knew him but briefly, Kurtis embraced me as a close friend. I am a better man for having known him, and the world is a better place having had him.

Table of Contents

List of Figures

Chapter 1 – Introduction

Influenza Structure and Life Cycle

Influenza viruses are members of the Orthomyxoviridae virus family (23). Their viral particles are enveloped, and their single stranded, negative sense genomic RNA is segmented (23). There are four major subtypes of Orthomyxoviridae: A, B, C and D (30). Influenza A and B are generally responsible for seasonal epidemics of flu in winter in the northern hemisphere (30). Newly emerging forms of influenza A that are differ substantially from previous strains can cause pandemics. Influenza C typically results in mild respiratory infections and is not thought to be associated with large-scale epidemics, while influenza D has thus far only been known to infect cattle (30). A typical influenza A virion has eight gene segments: HA, NA, PB1, PB2, PA, NP, NS, and M (13). These gene segments are contained within a viral capsid, composed of multiple different M proteins, which is contained within a viral envelope.

During infection, hemagglutinin (HA) on the virion surface binds to sialic acid on the epithelial cell exterior, triggering receptor mediated endocytosis and bringing the virus into the host cell within an endosome (23). As the pH drops inside the endosome, two key events occur: first, HA undergoes a conformational change, exposing a fusion domain that inserts itself within the endosome's membrane (23). Additionally, the matrix 2 (M2) ion channel opens and allows protons to flow into and acidify the viral core. This acidification causes matrix protein 1 (M1) to release viral ribonucleoprotein (vRNP), a complex of viral genomic RNA and nucleoprotein, NP, as well as polymerase protein subunits PA, PB1, and PB2, into the host cell cytoplasm (23).

Once in the cytoplasm, the vRNPs traffic to the nucleus thanks to the presence of nuclear localization sequences (NLSs) on each of its components (23). These NLSs can bind to the nucleus's import machinery. Following nuclear import, replication and transcription occur. Both these processes are accomplished with a viral RNA-dependent RNA polymerase (RdRp), imported as part of the vRNP complex – PA, PB1, PB2 (23). Replication proceeds when RdRp produces positive-sense RNA from genomic negative-sense RNA, which allows for the

production of new genomic negative-sense RNA (23). Furthermore, the positive-sense RNA generated by RdRp can serve as viral messenger RNA (mRNA) to enable the production of new viral proteins, with some modifications. Since viral transcription takes place inside the nucleus, viral mRNA requires 5' phosphate caps in order to be exported and targeted to the ribosome (23). Viral proteins are incapable of creating these caps, but they *are* quite effective at stealing 5' caps from host cell mRNAs (23). PB2 binds to host mRNAs and cleaves 5' caps, which prime RdRp to perform viral transcription through a mechanism known as cap-snatching. Production of poly-A tails occurs due to steric blockage of RdRp as it repeatedly transcribes short, 3' terminal poly-U genomic RNA sequences in a "stuttering" process (23).

While this mechanism of transcription is successful at producing mRNA for six of the gene segments, splicing is needed for segments M (which encodes for both M1 and M2) and NS (which codes for NS1 and NEP) (23). Host splicing machinery is inhibited from acting upon cellular mRNAs as NS1 binds to splicing components and is instead recruited to viral gene segments, where it splices the viral M and NS segments to allow for all encoded mRNAs to be produced. These spliced RNA products then undergo cap-snatching and polyadenylation through the mechanisms described above (23).

Once viral mRNAs possess the necessary 5' phosphate cap and 3' poly-A tail, they will then be exported from the nucleus and translated at the ribosome (23). As M1 is produced, it is brought into the nucleus to help mask an NLS present on vRNPs (23). NEP then binds to the NLS present on the M1 N-terminal domain, which allows for the complex to be exported from the nucleus (23). As HA, neuraminidase (NA), and M2 are translated they begin assembling into new viral particles at the apical side of infected epithelial cells. M1 bound to vRNPs will be packaged into the nascent virions. Ideally (for the virus) the forming virions will seal off once vRNPs for all eight gene segments are successfully incorporated (23). After packaging is complete the virus will then begin to bud from the plasma membrane of infected cells. Since the membrane enveloping the virus might contain sialic acid that could bind to neighboring virions'

HA, NA must cleave these residues to ensure successful release of the virus from the cell surface. After release from the apical surface of the infected cells, the new viral particles can then go on to infect neighboring cells (23).

Influenza A Host Tropisms and Evolution

Influenza A infection proceeds differently in reservoir and spillover hosts (31). Reservoir aquatic birds may experience asymptomatic or mild infections by influenza characterized by diarrhea. Mammalian hosts, including (but not limited to) humans, dogs and pigs typically suffer more severe symptoms that include respiratory distress, fevers and body aches (31). The transmission of newly evolved influenza A viruses (IAVs) from their natural aquatic fowl reservoirs to humans is thought to require (or at least benefit from) intermediate hosts, especially pigs (14). To understand why, a brief discussion of the structure of sialic acid, the cellular receptor recognized by IAV's HA protein, will be necessary.

Sialic acid present on the surface of airway epithelial cells is attached to penultimate galactose residues found on N-linked carbohydrates attached to proteins (11). This linkage occurs between the second carbon in the sialic acid ring and either the third or sixth carbon in the galactose ring-see figure 1.3 for a diagram of these linkages (11). Which carbon-linkage sialic acid possesses to the galactose causes it to be named, respectively, (2,3) or (2,6) sialic acid (11). These different bonds create a selective pressure for any IAV attempting to infect the associated species, since HA must be able to bind the present sialic acid to initiate endocytosis. Typically, human nasal epithelial cells carry much more (2,6) compared to (2,3) sialic acid on their surface (11). Most IAVs emerging from their reservoir host of aquatic fowl are adapted to the (2,3) sialic acid present on the surface of their epithelial cells, while human viruses must recognize (2,6) sialic acid present on our epithelial cells (14). Therefore, avian viruses have a difficult time infecting human nasal epithelial cells compared to human-adapted viruses. However, pigs' nasal epithelial cells express both (2,3) and (2,6) sialic acid, which enables them to be infected by

influenza viruses originating from water fowl and human hosts (14). This can present (2,3) adapted IAVs originating from birds the opportunity to mutate and recognize (2,6) sialic acid, thereby becoming infectious to humans.

Such adaptations can occur in one of two ways – mutation or reassortment – both of which occur due to the segmented nature of influenza's RNA genome (32). Mutation, or genetic drift, results from erroneous additions of nucleotides to newly forming genomic viral RNA strands during replication (32). The error rate of influenza A RdRp, which has no proofreading function, is roughly equivalent to 1 per genome produced (10). Since many thousands of genomes can originate from a single infected cell, this means that many mutations can accumulate in a single individual infected with IAV that can then be transmitted to the next host, where new mutations can compound already existing ones before being passed to the next host, and so on (10). These drift mutations can give rise to strains of influenza circulating between different influenza outbreak seasons.

The second way mutations can occur within influenza genomes is called reassortment, or antigenic shift (32). During viral particle packaging, vRNPs with each of the eight IAV gene segments are loaded into nascent virions. While there is some evidence that this occurs in a specific manner so that multiple copies of the same gene segment are not usually loaded into the same virion, there is no requirement that all of the vRNP gene segments in any given virion must originate from the same parental virus (23). If an epithelial cell were infected with two or more strains of influenza simultaneously, then some viral particles would by chance possess gene segments from each of the parental strains. These new combinations of gene segments can produce viruses against which hosts have no immunity. Depending on the virulence of the new strains and their transmissibility, this can give rise to pandemics (32). Returning to the discussion of sialic acid momentarily, gene segment reassortment between avian and human influenza gene segments could occur within pigs thanks to their possession of both (2,3) and (2,6) sialic acid

(14). Reassortment is the mechanism that is believed to have given rise to the 2009 influenza pandemic strain (18).

Vaccinating Against IAV

Reassortment events and drift mutations are critical to influenza's ability to evade antibodies against previous years' strains. Typically, human anti-influenza antibodies form against HA (28). Binding of antibodies to HA protects cells from infection by preventing the virus from binding to sialic acid. Antibodies can also form against NA, which blocks newly budding viral particles from successfully exiting host cells by preventing the cleavage of sialic acid from HA (28).

Vaccines against influenza virus begin production months before the flu season begins. How these vaccines are made is determined by what flu viruses were prominent during the previous year's flu season, which provides information about what circulating strains might be most likely to emerge as dominant in the future (12). Special attention is paid to the HA and NA proteins of these likely-dominant viruses since the immune system typically produces antibodies against them. Production of vaccines begins by generating viruses with the desired combination of HA and NA genes (7). Critically, these viruses must be capable of infecting embryonated hen's eggs, the current standard for growing large quantities of vaccine stock. Once eggs are injected, and viruses replicate to immunogenic titers, the viruses are harvested from the eggs (7). There are, however, some issues with this method of developing vaccines; one of the possible consequences is vaccine mismatch.

Vaccine mismatch can result from the vaccine manufacturing process itself. Since hens' eggs are used to culture vaccine strains of influenza, the virus is under selective pressures unique to replicating within the eggs (28). These pressures would be absent within the human host, which could result in mutants with traits favorable to the egg host outcompeting the desired vaccine strain originally injected into the egg. Then, when the virus is harvested from the eggs,

its protein epitopes might not be identical to the ones found in the naturally circulating strains (28). Any antibodies made against the egg adapted vaccine strains might be less effective against the seasonal strains as a result (28).

Another problem with developing vaccines in hens' eggs is time. Egg procurement, viral growth, and the harvesting, preparation and testing of vaccines all need time to complete (7). This process takes months, and the vaccine produced cannot readily be adapted if the dominant circulating seasonal influenza strains mutate during the time it takes to produce the vaccine. Any mutations, whether they be drift mutations in the gene segments themselves that result in protein epitope changes or reassortment events that produce new influenza A viruses altogether, might alter the immunogenic epitopes of the circulating seasonal flu such that the antibodies elicited by immunization have little to no protective effect (7).

Seasonal Influenza Outbreaks in the United States, 2016-17 and 2017-18

The 2016-17 influenza outbreak in the U.S. was dominated by influenza A viruses of the H3N2 subtype (8). Compared to past outbreaks, the 2016-17 season was relatively mild, with numbers of cases consistent with recent seasons. During the 2016-17 season, the dominant circulating strains of IAV belonged to the H3N2 clade 3C.2a1 (3). The vaccine strain deployed in the 2016-17 season included influenza A H3N2 3C.2a Hong Kong, which seemed relatively effective at controlling the number of cases of influenza.

For the 2017-18 influenza season, the Hong Kong derived vaccine strain was again employed as the H3N2 component (2). Influenza A subtype H3 accounted for the majority of cases in the 2017-18 flu season just as it did in the 2016-17 season (3). This suggests that the IAV H3 Hong Kong vaccine was still poorly protective against H3N2 strains circulating in the United States in the 2017-18 season. Figure 1.4 shows that there were more cases of influenza-like illness reported to outpatient clinics in the 2017-18 season as compared to 2016-17 (3). Correspondingly, the 2017-18 season found more patients hospitalized with influenza-like illness

than the 2016-17 season (8). The IAV H3N2 Hong Kong derived vaccine was used in both seasons, yet cases of and hospitalizations from influenza-like illness were both significantly higher in the 2017-18 season (8). If the vaccine were equally as ineffective in both seasons, we would not expect to see such a large difference in the number of cases or hospitalizations. Something must have changed about influenza between the 2016-17 and 2017-18 seasons that can account for the observed increase in transmissibility and virulence.

A Novel Reassortment Event Between Two Influenza A H3N2 Clades

Earlier, two ways in which IAVs can mutate – genetic drift and reassortment – were discussed. (32). Typically, drastic increases in transmissibility and virulence like those observed between the 2016-17 and 2017-18 seasons occur when there is a reassortment event that significantly alters the circulating viruses, as was believed to have occurred during the 2009 pandemic influenza season (18). Reassortment is uncommon for several reasons. First, a host cell must be infected with multiple different strains of IAV simultaneously. Second, gene segments from different IAV parental viruses must randomly be incorporated into a nascent virion. Third, any virions produced by the reassorted gene segments must successfully be able to exit their host cell and infect new cells. Should these conditions be met, reassortant IAVs could be quite phenotypically distinct from any parental viruses from which they were derived, resulting in the ability to infect new host organisms, evade extant antibodies within their host populations, replicate more rapidly, spread more easily, cause greater morbidity and potentially mortality in their host species.

Between the 2016-17 and 2017-18 flu seasons in the United States there was a reassortment event between viruses of different H3N2 clades. The schematic for these reassortments is shown in figure 1.1 (manuscript in progress).

During the 2016-17 influenza season, three viral clades of H3N2 circulated with no evidence of any reassortment between their genomes: 3C.2a1, 3C.2a2 and 3C.3a. (4). In the 2017-18 flu season, 3C.2a1 gene segments identified by sequencing were found in circulating 3C.2a2 and 3C.3a viruses, which suggested that reassortment had occurred between viruses of these clades. Specifically, 3C.3a viruses isolated within the Johns Hopkins Centers for Excellence in Influenza Research and Surveillance (JH CEIRS) during the 2017-18 season contained five 3C.2a1 gene segments (PB1, PB2, PA, NP and NA) and three 3C.3a gene segments (HA, M, and NS), referred to as a 5:3 reassortment (manuscript in progress). 3C.2a2 viruses also underwent a reassortment event, combining six 3C.2a1 gene segments (PB2, PA, NP, NA, M, and NS) with two 3C.3a gene segments (PB1 and HA), or a 6:2 reassortment (manuscript in progress). The 5:3 reassortant 3C.3a viruses isolated in the 2017-18 flu season were the focus of this thesis work, while a post-doctoral member of the lab, Dr. Jason Westerbeck, studied 3C.2a2 viruses.

Hypothesis and Research Aims

Based on the enhanced severity and number of cases associated with the 2017-18 U.S. influenza season, it was hypothesized that the 3:5 reassortment event between the 3C.3a and 3C.2a1 clades conferred the reassortant viruses with increased viral fitness compared to the circulating 3C.2a1 viruses from the 2016-17 outbreak, which could have been responsible for some of the increased transmissibility and virulence noted in the 2017-18 outbreak. To test this hypothesis, work centered on these specific research aims:

1. Phenotypic characterization of the 3C.2a1 and 3C.3a viruses circulating in the 2016-17 season and the 3C.3a viruses collected in the 2017-18 season. This aim will be the topic of chapter two.
2. Generating and phenotypically characterizing recombinant viruses through cloning that represented different combinations of reassorted gene segments from the 3C.2a1 and 3C.3a viruses to determine which segments contributed significantly to the phenotype of the reassortant 3C.3a viruses. This aim is discussed in depth in chapter three.

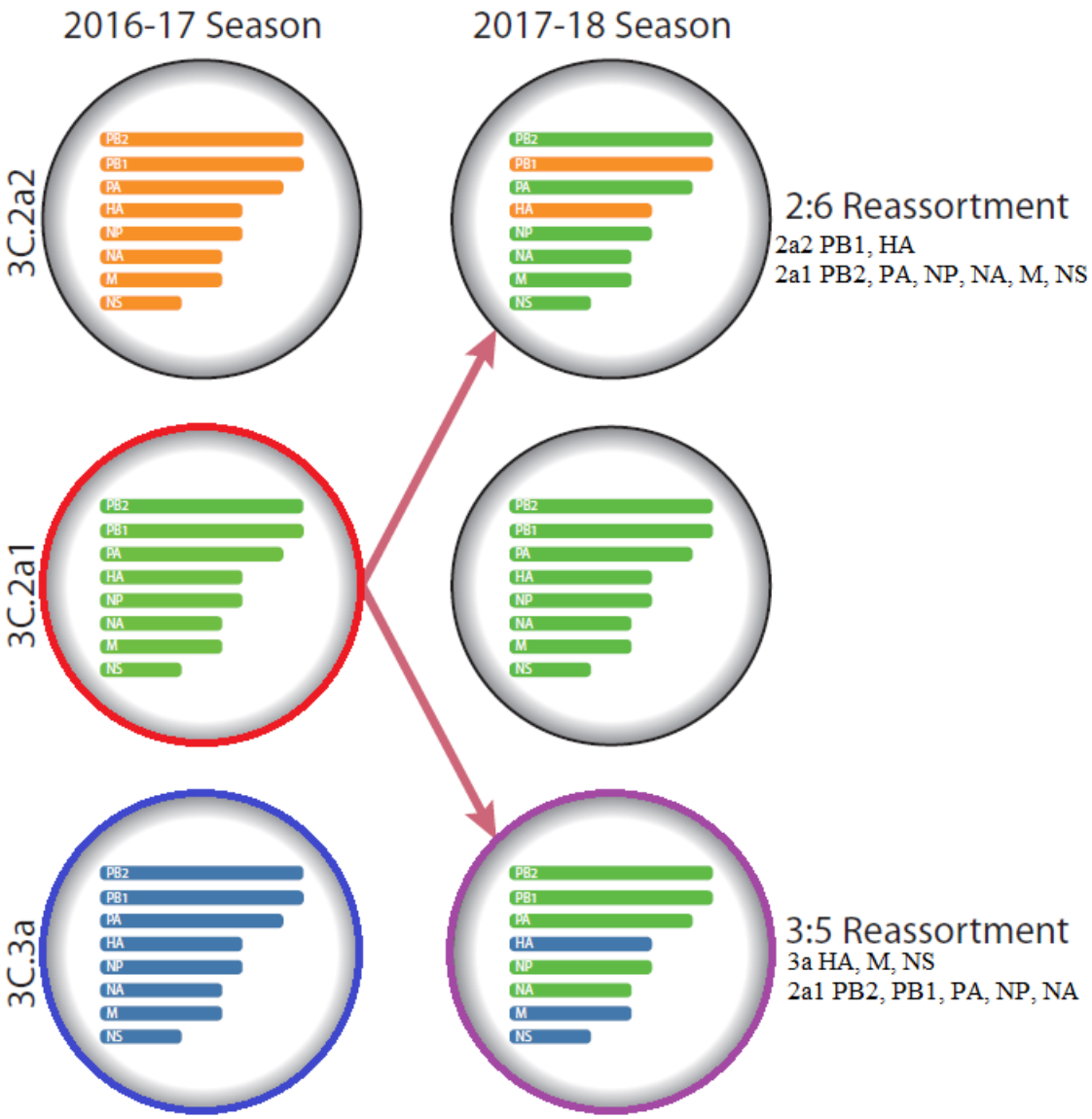

Figure 1.1
During the U.S. 2016-17 seasonal outbreak of influenza, circulating strains of H3N2 influenza could be classified 3C.2a1, 3C.2a2 and 3C.3a clades. Between the 2016-17 and 2017-18 seasons, two reassortment events occurred: the 3C.2a2 HA and PB1 gene segments reassorted into a 3C.2a1 background. Separately, 3C.3a HA, M, and NS reassorted into a 3C.2a1 background.

Chapter 2 – Phenotypic Characterization of Clinically Isolated Viruses

Experimental Rationale

These experiments aimed at elucidating two phenotypic characteristics of influenza A viruses – replication kinetics following infection and morphological differences in viral plaques in monolayer cultures.

Replication rate is a useful proxy for viral fitness since it shows how rapidly different viral strains are reproducing in culture following infection with an identical initial concentration of virus. Any differences in viral titers in supernatants collected from cells infected with different viruses, assuming that the initial doses were identical, can be said to be due to characteristics intrinsic to the viruses themselves. Thus, if one strain or clade replicates more rapidly consistently than another, this is suggestive that the more rapidly replicating virus might possess an advantageous phenotype – which, in turn, could help explain the seasonal differences observed with the increase in virulence of the 2017-18 season compared to 2016-17. In this chapter, growth curves on both primary human nasal epithelial cells (hNECs) and MDCK-Siat cells, followed by $TCID_{50}$ on MDCK-Siats, were used to determine which viruses experienced more rapid replication kinetics.

Plaque morphology is another proxy for viral fitness. Plaques, or areas on culture plates with predominantly dead cells, form as a single virus infects a single MDCK cell, replicates within it, and infects nearby cells as progeny viruses bud from the originally infected cell. An agar overlay ensures that viruses cannot freely diffuse through liquid media following budding and must infect adjacent cells. Viruses that replicate and bud from cells more rapidly will infect adjacent cells at a higher rate than slower replicating strains, producing larger plaques. Therefore, plaque size is a proxy for how well viruses spread through environments where they cannot float freely through permissive aqueous media. Since human nasal passages are coated in thick mucus that can block viral movement from one cell to the next, the plaque assay can provide a better understanding of how viruses behave in that kind of restricted environment.

Materials and Methods

Common Cell Lines

Experiments with viruses were conducted across four different cell types: MDCKs, MDCK-Siats, hNECs and 293T cells. MDCK, short for Madin-Darby Canine Kidney cells, are immortalized canine kidney epithelial cells useful for their relative ease in culturing and susceptibility to influenza infection due to the presence of both (2,3) and (2,6) linked sialic acid (15). MDCK-Siat cells are MDCK cells that express two-fold higher levels of (2,6) sialic acid compared to MDCK cells (15). This results from a successfully maintained transfection of human alpha-2,6-sialyltransferase cDNA into MDCK cells (15). Because the (2,6) linkage mirrors what is present in human nasal epithelial cells (hNECs) MDCK-Siat cells should be a good immortalized cell model for infection. When possible, it was preferable to work with MDCK-Siat cells as compared to hNECs, since hNECs required greater maintenance and had to be acquired directly from human subjects.

Experimental protocols for MDCK and MDCK-Siat cells were generally interchangeable. For abbreviation purposes, if cells of either type are referred to nonspecifically in a protocol, the shorthand "MDCK/Siat" will be used.

Common Reagents

The following is a list of common reagents used across experiments in chapters 2 and 3 for ease of reference.

- Phosphate-Buffered Saline (PBS): Saline solution that includes dissolved phosphate, generally employed as a means to wash cells during passaging.
- Phosphate-Buffered Saline with .1% by volume calcium and magnesium (PBS+): PBS supplemented with calcium and magnesium ions that help fix cells to wells in plates.

- Dulbecco's Modified Eagle Media (DMEM): DMEM contains glucose, vitamins and amino acids essential for cellular growth. It includes sodium bicarbonate as a pH indicator. (Yao, 2017)
- Complete DMEM: DMEM that includes 10% by volume fetal bovine serum (FBS) and 1% by volume each of the antibiotics glutamax (G) and penicillin/streptomycin (P/S).
- Infectious Media (IM): DMEM that includes 1% by volume each of the antibiotics glutamax (G) and penicillin/streptomycin (P/S), and immediately prior to infection will typically be fortified with 1% by volume of 30% bovine serum albumin (BSA) and .1% or .2% by volume N-acetylated-Trypsin (NAT).
- Trypsin: A lab stock of the enzyme trypsin, which is diluted 1:5 with PBS when needed to resuspend cells in fresh media during culture passage.
- Paraformaldehyde: A lab stock of paraformaldehyde, which was diluted to 4% in PBS to fix cells following an infection for analysis.
- Naphthol Blue Black: A dye mixed with glacial acetic acid, PBS, sodium-acetate to stain fixed cells following fixation with paraformaldehyde.

Virus Strains Studied

Initial growth curve experiments were conducted with one virus from the 3C.2a1 clade isolated during the 2016-17 season (R0145), one virus from the 3C.3a clade also acquired in the 2016-17 season (0244), and one reassortant 3C.3a virus from the 2017-18 season (R0230). In order to better understand the phenotypic changes between the reassortant 3C.3a circulating in the 2017-18 season compared with parental 3C.3a and 3C.2a1 strains isolated in 2016-17, one additional virus from each clade was selected for further study, bringing the number of viruses per clade to two. These viruses are summarized in the table provided in figure 2.1.

Maintaining MDCK/Siat Cells

The basic technique of maintaining MDCK/Siat that follows is similar to the methods employed by Dr. Abdoli and his collaborators (15). MDCK/Siat cells were split once every three to four days. Splitting begins by washing MDCK/Siat cells with PBS, followed by suctioning of suspended cells. 5 mL of trypsin, diluted by a factor of 1:5 in PBS, was then pipetted onto the surface of the cell monolayer and incubated at 37 C for 20 minutes. Following trypsinization, 5 mL of complete DMEM would be added and pipetted up and down repeatedly to completely remove cells from the surface of the flask. 1 mL of cells, trypsin and DMEM would be left in the flask, and approximately 20 mL of DMEM would be added to allow the MDCK/Siat cells to repopulate. The remaining 9 mL of cells could be used to prepare for future experiments or discarded if not needed.

MDCK/Siat Low MOI Growth Curves

Growth curves began by seeding MDCK/Siat cells onto 24-well plates at concentrations of $5x10^5$ cells/well and incubating the plates at 37 C for sixteen hours. Viruses would be diluted to an MOI of 0.001 through serial dilution on 96 well plates. Following dilution, the 24-well plates bearing MDCK/Siat cells would be washed with PBS+ to ensure cell adhesion to the well. 100 μL of each diluted virus would be pipetted into the appropriate wells, with each virus being grown in triplicate to generate three technical replicates. A mock infection, consisting of infectious media prepared for the experiment that lacked virus, was also carried out in triplicate. The remaining inoculum would be saved at -80 C for verification that input concentrations of each virus were similar.

Following infection, the 24 well plates would be rocked on an automatic plate rocker for one hour at room temperature to allow an even distribution of virus across the surface of the MDCK/Siat monolayer. The viral media would then be aspirated and 500 μL of fresh infectious media would be applied to each well. The 24 well plates would then incubate at 32 C for the

remainder of the experiment. Supernatants would be collected at 1, 12, 24, 36, 48 and 72 hours after this initial change in media. Each time, fresh infectious media would be supplied to the cells to capture newly budding viral particles.

After a growth curve was completed, the replication phenotype of the viruses at the different timepoint samples collected was characterized through a median tissue culture infectious-dose ($TCID_{50}$) assay.

$TCID_{50}$ Assay

First, MDCK/Siat cells would be seeded into 96 well plates at a concentration of $1x10^5$ cells/well and incubate at 37 C for three days. These seeded plates then were washed twice with 100 µL of PBS+ and 180 µL fresh infectious media applied. Until needed for infection plates were kept at 32 C. Supernatant samples from the growth curves would then be serially diluted from their initial concentrations by factors of ten, from $1x10^{-1}$ to $1x10^{-8}$ in round-bottom 96 well plates. 20 µL of each diluted supernatant sample would then be pipetted to the appropriate wells of the MDCK/Siat seeded 96 well plates and incubated at 32 C for six days. At the end of the incubation period, 75 µL of 4% paraformaldehyde would be added for three or more hours to each well to fix cells. After decanting the media and paraformaldehyde, 100 µL of Naphthol Blue-Black stain would be added to each well for three or more hours. Plates would then be washed with water and examined to quantify viral titers.

Plaque Assay

MDCK cells were used to examine differences in plaque morphology between the viruses in figure 2.1. After trypsinization during splitting, 2.5 mL of MDCK cells would be seeded in 6 well plates at a concentration of $5x10^5$ cells/well. To ensure uniform distribution of cells, the plates were gently rocked by hand after seeding. Plates were then incubated overnight at 37 C. Once confluent within their wells, the MDCK cells would be washed twice with PBS+. After the

wash step, 1 mL DMEM with P/S and G would be added to each MDCK well and the 6 well plates would be stored at 32 C until needed.

24 well plates were used to dilute viral working stocks in preparation for infection. 720 µL infectious media was added to each well of the 24 well plate. Into the first well, 80 µL of viral working stock would be added and mixed via pipetting, and 1:10 serial dilution would be carried out so that the final well would have a concentration $1x10^{-6}$ of the initial working stock. After removing the DMEM from the MDCK seeded plates, diluted virus would be added to the appropriate MDCK wells. Once infection began, the plates were incubated at 32 C for one hour with gentle agitation every fifteen minutes to distribute the virus evenly throughout the wells.

During the hour incubation 2x DMEM media (containing twice the concentration of reagents found in DMEM, twice as much antibiotic as used in infectious media, and 10 mL of HEPES) was made and 2% agarose solution was microwaved, then stored in a 67 C water bath. At the end of the incubation step, viral media was aspirated from the 6 well plates and 2x DMEM and 2% agarose were mixed in a 1:1 ratio to generate 1% agarose DMEM media. 3 mL of 1% agarose DMEM media was applied to each well, and the 6 well plates were incubated in 32 C for three days or until plaques became visible to the naked eye. Once plaques could be seen, 1 mL of 4% paraformaldehyde was added per well for four or more hours, after which the agar overlay was removed. 1 mL of Naphthol Blue-Black dye per well was added to the exposed cells for no more than 1.5 hours, after which the dye would be washed off and plaque size quantified.

Quantification of Plaque Assays

To quantify plaque size and morphology, images taken of each 6 well plate via light dissection microscopy were examined to identify the highest concentration where wells had not been completely cleared of cells by the viruses. Then, using the ImageJ software's hand-drawn region of interest selection tool, plaques and areas immediately surrounding plaques where partial clearance was observed were circled. If two plaques were adjacent to each other, a best

approximation of the size and shape of the plaque would be made based off of estimated plaque radius. Plaques that abutted the edge of the well were not selected for quantification.

hNEC Cell Maintenance

Human nasal epithelial cells (hNECs) were obtained from a collaborating lab that harvested them directly from human volunteers. Upon receipt of the cells, fresh ALI media would need to be provided to the basolateral component of the well once every other day. This replacement of media provided fresh nutrients to the hNECs. Prior to their usage in growth curve experiments, hNEC wells would be monitored for potential contamination. Any contaminated wells would be discarded prior to the commencement of any growth curve experiments.

hNEC Growth Curves

DMEM infectious media without any N-acetylated trypsin was prepared for hNEC growth curves. Viral dilution to an MOI of 0.01 was achieved via serial dilution on 96 well plates. Prior to infection, fresh ALI media was supplied to the basolateral surface of the hNEC wells and the apical surface was washed twice with the hNEC infectious media, leaving the cells covered in wash media for five minutes in 32 C prior to aspiration. After washing, 50 μL of virus from the inoculum sample was then applied to the apical surface of the hNECs, and the plates were incubated for two hours at 32 C.

Following infection and initial incubation, viral media was aspirated. At timepoints 1, 12, 24, 36, 48, 72, and 96 hours following the end of the initial two hour incubation, 100 μL of infectious media would be applied to the apical surface of the hNEC wells and the plates would be incubated at 32 C for ten minutes. The infectious media would then be collected and stored at -80 C until needed for $TCID_{50}$ assay. At 48 and 96 hours post infection, ALI media from the basolateral surface would be collected, stored at -80 C and replaced with fresh media.

Flow Cytometry

While growth curves and plaque assays could determine replication kinetics of the viruses under study, they were not well suited to characterize how efficiently viruses infected cells. To study that question, flow cytometry was conducted on hNECs infected (according to the protocol outlined in the above section) by the six viruses in duplicate wells for 16 hours incubated at 32 C. At the end of 16 hours the hNECs were trypsinized and pelleted via centrifugation into individual 15 mL conical tubes, where they were fixed with 2% paraformaldehyde. Following fixation the cells were then resuspended and transferred to FACS tubes and washed twice with PBS. Permeabilization buffer (0.2% by volume Tween-20 dissolved in FACS buffer, 0.3% BSA in PBS) was then added and cells were incubated with the buffer for 15 minutes at room temperature. Following a wash with FACS buffer, the cells were then incubated for 30 minutes at room temperature with blocking buffer added. Once washed again with FACS buffer, half of the experimental tubes would be exposed to both beta-tubulin and human anti-serum isolated from patients in the 2016-17 outbreak containing polyclonal antibodies against 3C.2a1 viruses circulating at the time. The other half of experimental tubes would only be inoculated with beta-tubulin. Both halves needed to be incubated for 20 minutes at room temperature, then washed with FACS buffer. Goat serum containing anti-mouse IgG antibodies (goat anti-mouse IgG AF 488) and goat serum with anti-human IgG (goat anti-human AF647) were then added to all experimental tubes and incubated for 20 minutes at room temperature. Following another FACS wash, EpCAM-PE (an antibody against epithelial cell epitopes present on the surface of epithelial cells) was added to each experimental tube and incubated for twenty minutes. Tubes were then washed with FACS buffer and run on the flow cytometer.

Results

Initial Low MOI Growth Curves

The phenotypic effects that reassorting the 3C.3a 2016-17 gene segments HA, M and NS into a 3C.2a1 background had on virus replication were first characterized by low multiplicity of infection (MOI=0.001) growth curves. It was unknown which cell type would better permit the clinically isolated 3C.2a1 and 3C.3a viruses from the 2016-17 and 2017-18 U.S. flu seasons to replicate. To determine this, initial growth curves were done in both MDCK and MDCK-Siat cells. At first, $TCID_{50}$ assays were only carried out on the inoculum and 72 hours post infection (HPI) timepoint; if there was no virus present at 72 HPI despite being detected in the inoculum, there would be no need to measure titers of time points before 72 HPI. Figure 2.2 shows the $TCID_{50}$ results for the first MDCK growth curve conducted on the inoculum and 72 HPI samples.

At an MOI of 0.001, none of the viruses applied to MDCK cells showed infectious particle production after 72 hours (Figure 2.2). However, $TCID_{50}$ assays showed that the same viruses at the same MOI infecting MDCK-Siat cells could replicate at 72 HPI (figure 2.3). These experiments demonstrated that MDCK cells seemed refractory to infection with this panel of viruses, so MDCK-Siat cells were chosen for more extensive analysis of viral replication. Furthermore, the initial $TCID_{50}$ data on MDCK-Siat cells seemed to suggest that 3C.3a viruses replicated better than 3C.2a1 viruses, and that the 3C.3a reassortant from 2017-18 replicated to higher titers faster than the 3C.3a parental virus from 2016-17.

MDCK-Siat Growth Curves with more clinical isolates

The initial MDCK and Siat growth curves were only performed with one virus from each clade. To more definitively characterize the phenotypic differences between the clades, more viruses and repeated experiments were needed. Multiple clinical isolates of H3N2 influenza A viruses isolated from Baltimore patients during the 2016-17 and 2017-18 outbreaks, including

several viruses of both clades 3C.2a1 and 3C.3a, were available for study. Two viruses from each clade (see figure 2.1) were selected for all future experiments.

Three separate low MOI=0.001 MDCK-Siat growth curve experiments were conducted with these six viruses, with each virus undergoing three technical replicates in each experiment (figure 2.4). The results of each growth curve's $TCID_{50}$ are shown in panels A, B and C. Panel D collapsed data across all three growth curves. Each experiment showed the similar trends to those present in the initial MDCK-Siat growth curve; 3C.3a parental and reassortant viruses replicated to higher viral titers with faster kinetics than 3C.2a1 viruses. However, the 3C.3a reassortant viruses did not replicate to higher titers or with faster kinetics than 3C.3a parental viruses.

hNEC Growth Curves

MDCK-Siats are immortalized kidney epithelial cells, and therefore, not a typical cell line that influenza would encounter in the course of a natural infection. To ensure the phenotypes observed in the MDCK-Siat cells were not anomalous, it was important to perform growth curve experiments in hNECs isolated from healthy individuals. Figure 2.8 summarizes the hNEC growth curve experiments conducted thus far to characterize the panel of clinically isolated viruses selected for this research. The phenotypes observed in the hNECs were consistent with the work conducted in MDCK-Siat cells, indicating that these viruses behaved similarly and, therefore, that the observed phenotype in the MDCK-Siat cells was conserved in a primary epithelial cell culture system.

Plaque Morphology Characterization

To characterize the differences in plaque morphology between the panel of viruses under study, MDCK cells, which are permissive for plaque formation with 2016-17 H3N2 viruses despite the fact that they do not support the production of infectious virus (see Figure 2.2), were used. Three plaque assays were performed, with each virus having two technical replicates per

assay. The results of the individual plaque assay replicates are displayed in figure 2.6, panels A, B and C. Panel D collapses the data across all three experiments. Panels E, F and G are representative images of the indicated viral clades.

Figure 2.7 summarizes the data from the collapsed analysis of all three biological replicates. 2016-17 3C.3a parental viruses exhibited plaque size area 50% greater than 2016-17 3C.2a1 parental viruses, while 2017-18 3C.3a reassortant viruses produced plaques 85.5% greater in size than 3C.2a1 parentals. Within the 3C.3a clade, the reassortants produced plaques 23.7% larger than parentals.

Flow Cytometry

Figure 2.8 summarizes the results of the initial flow cytometry experiment. No statistically significant differences were detected between the viral clades with regard to the percentage of cells, epithelial cells, or ciliated epithelial cells infected.

Discussion

MDCK cells are used throughout the Pekosz laboratory as a typical cell-line for growth curves, $TCID_{50}$s, and plaque assays. It was unusual that the IAVs isolated from the 2016-17 and 2017-18 seasons seemed unable to effectively infect MDCK cells at low MOIs associated with growth curves. Following the initial growth curves in both MDCK and MDCK-Siat cells, growth curves in immortalized cells were conducted exclusively on MDCK-Siat cells.

The initial MDCK-Siat growth curve (Figure 2.3) suggested that there was a measurable phenotypic difference in replication rates of 2016-17 3C.2a1 compared to both 2016-17 parental and 2017-18 reassortant 3C.3a viruses, and even between the parental and reassortant 3C.3a viruses. For training purposes, these initial growth curves were only conducted with one virus from each clade. To garner more statistical power for future analysis, subsequent growth curves included two viruses each clade (Figure 2.1).

As figure 2.4 demonstrates, the phenotypic differences between 2016-17 3C.2a1 viruses and 3C.3a viruses from both 2016-17 and 2017-18 were consistent throughout biological replicates. In each experiment, the 3C.3a parental and reassortant viruses always grew more rapidly to higher titers than the 3C.2a1 viruses. Unlike the initial MDCK-Siat growth curve, the 2017-18 3C.3a reassortant viruses did not exhibit a clear replication advantage compared to the 2016-17 parental 3C.3a viruses. In each biological replicate and after collapsing across all three, there was no statistically significant difference at two or more time points between the 3C.3a reassortant and 3C.3a parental viruses (Figure 2.4).

Analysis of the hNEC growth curve experiments returned similar results – there were never consistent differences between the 2016-17 and 2017-18 3C.3a viruses, while both the reassortant and parental 3C.3a viruses grew more rapidly than 3C.2a1 viruses (Figure 2.5). Since hNECs represent a model closer to actual infection of a human than MDCK or MDCK-Siat cells, their results are considered a gold standard in the Pekosz laboratory. Therefore, agreement between the hNEC and MDCK-Siat results bolstered the significance of the MDCK-Siat findings and meant that, in future experiments, results in MDCK-Siat cells would likely represent what would be observed in hNECs – at least for these H3N2 strains.

Given the difficulty in growing these viruses on MDCK cells during the initial growth curve experiments, there was some concern regarding whether plaque assays would be successful since they must be conducted with MDCK cells. However, as Figure 2.6 shows, plaque formation within MDCK cells was successful. This is potentially because plaque assays measure the spread of viruses to neighboring cells (cell-to-cell spread) while growth curves measure the release of infectious virus particles. MDCK cells maintain the ability to support cell-to-cell spread of 2016-17 H3N2 viruses and, therefore, can be used to study plaque formation.

By eye, the plaques formed by 3C.2a1 parental viruses appeared smaller than those produced by either parental or reassortant 3C.3a viruses (Figure 2.6, panels E, F and G). Results of plaque morphology quantification via ImageJ agreed with conclusions from MDCK-Siat and

hNEC growth curve data – 3C.3a viruses isolated from the 2016-17 and 2017-18 seasons generated larger plaques than 3C.2a1 viruses from the 2016-17 season. Interestingly, the 3C.3a reassortants from 2017-18 produced plaques across all three experiments that were about 23% larger on average than the 2016-17 3C.3a parental viruses. Given the inability of all three biological replicates of the plaque assay to capture this phenotypic difference between the reassortant and parental 3C.3a viruses, it would be difficult to draw any conclusions about fitness differences of the parental and reassortant 3C.3a viruses based on these MDCK plaque assays alone, especially since these data seemingly contradict the results from the gold standard hNEC growth curves (figure 2.5). Nevertheless, since growth curves measure viral release into supernatant from infected cells, and plaque assays quantify how rapidly viruses can spread between adjacent cells, the results in figures 2.6 and 2.7 might be indicating that 3C.3a reassortant viruses from the 2017-18 season are capable of initiating cell-to-cell infections more rapidly than either the 3C.3a or 3C.2a1 parental strains.

The initial flow cytometry experiment sought to determine whether the advantageous replication phenotype observed in the 3C.3a viruses as compared to the parental 3C.2a1 viruses might be due to the efficiency of infection of cells of each virus. Each of the panel of viruses under study was used to infect hNECs in duplicate for 16 hours. After collecting and processing cells, they were run on a flow cytometer and the results quantified via FlowJo. Figure 2.8 summarizes the efficiency of infection of each virus on total cells present in the samples (panel A), epithelial cells (panel B), and ciliated epithelial cells (panel C). There were no statistically significant differences between the efficiency of infection between viruses of different clades across the three cell types probed. Since this is only a single replicate, it is premature to conclude that 3C.3a viruses from the 2016-17 and 2017-18 U.S. flu seasons do not infect cells more or less efficiently than 3C.2a1 viruses from the 2016-17 outbreak – this phenotype must be confirmed with further replicates.

In summary, 3C.3a viruses from both the 2016-17 and 2017-18 U.S. flu seasons replicated more rapidly to higher titers than 3C.2a1 viruses isolated in the 2016-17 outbreak, in both MDCK-Siat and hNEC growth curves. Furthermore, 3C.3a viruses generated larger plaques than 3C.2a1 viruses, and there was a statistically significant difference between the plaque sizes of 3C.3a parental and reassortant viruses when collapsed across all three replicates. Flow cytometry indicated no difference in efficiency of infection between the viruses under study, though more replicates will be needed before any conclusions may be drawn.

Virus I.D.	Clade	Season Isolated
Baltimore 0244	3C.3a	2016-2017
Baltimore R0096	3C.3a	2016-2017
Baltimore R0145	3C.2a1	2016-2017
Baltimore 0284	3C.2a1	2016-2017
Baltimore R0230	3C.3a reassortant	2017-2018
Baltimore R0243	3C.3a reassortant	2017-2018

Figure 2.1
Six clinically isolated viruses were used to characterize phenotypic differences between the 2016-17 3C.2a1, 3C.3a, and the 2017-18 3C.3a clades. These viruses were obtained from patients in treatment at the Johns Hopkins Hospital through the Center of Excellence for Influenza Research and Surveillance (CEIRS).

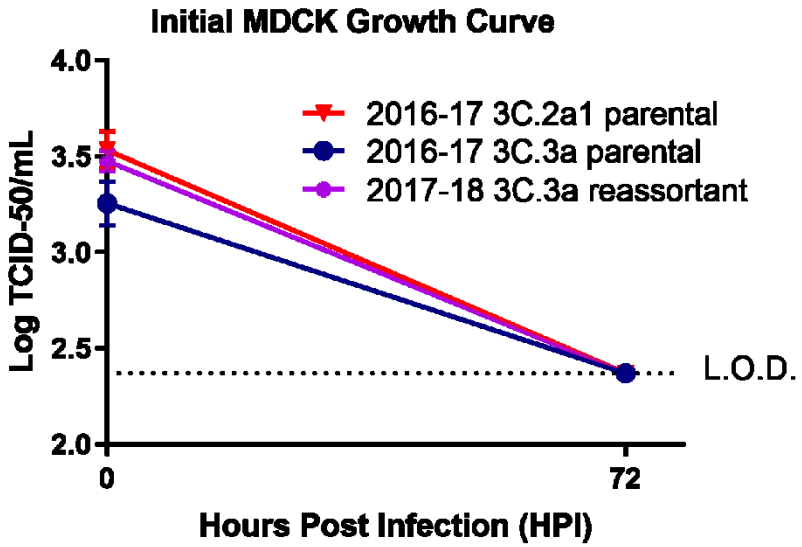

Figure 2.2
One virus from each clade (2016-17 3C.2a1, 2016-17 3C.3a, 2017-18 3C.3a) was used to infect MDCKcells at a low MOI of 0.001. Each virus in this growth curve had three technical replicates. The 72 hour post infection (HPI) timepoint was titered to determine if these viruses could infect MDCK cells. No viral replication was detected in the 72 HPI samples.

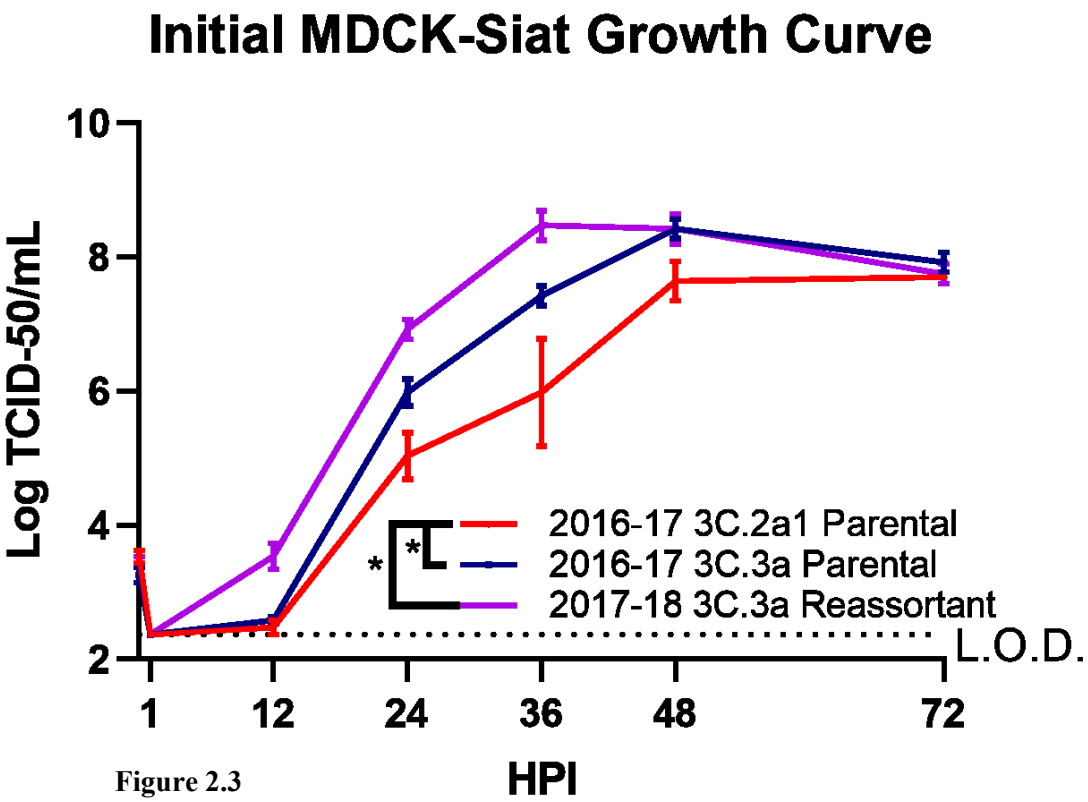

Figure 2.3
One virus from each clade (2016-17 3C.2a1, 2016-17 3C.3a, 2017-18 3C.3a) was used to infect MDCK-Siat cells to determine if there were detectable phenotypic differences between clades. Each virus in this growth curve had three technical replicates.
Asterisks denote statistically significant differences ($p<0.05$) at two or more timepoints in a multiple-comparisons, two-way ANOVA between the clades indicated by the brackets. Error bars represent standard error of means (SEM).

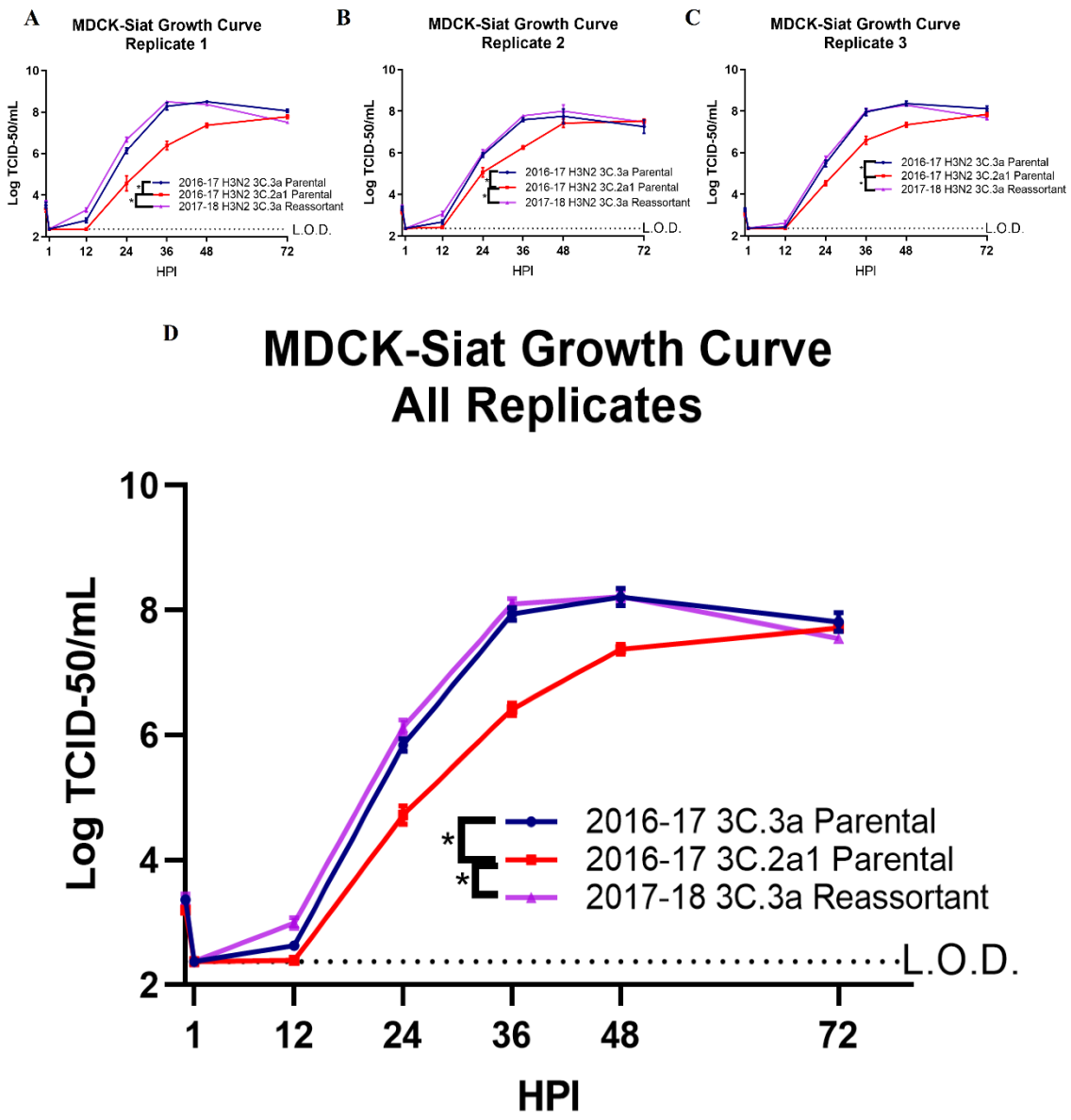

Figure 2.4
Two viruses from the three clades under study (2016-17 3C.2a1, 2016-17 3C.3a and 2017-18 3C.3a) were used to infect MDCK-Siat cells in low MOI (0.001) growth curves. Each individual growth curve (panels A, B, and C) had three technical replicates for each virus. Panel D shows the data from all three growth curves collapsed into a single graph.
Asterisks denote statistically significant differences ($p<0.05$) at two or more timepoints in a multiple-comparisons, two-way ANOVA between the clades indicated by the brackets. Error bars represent standard error of means (SEM).

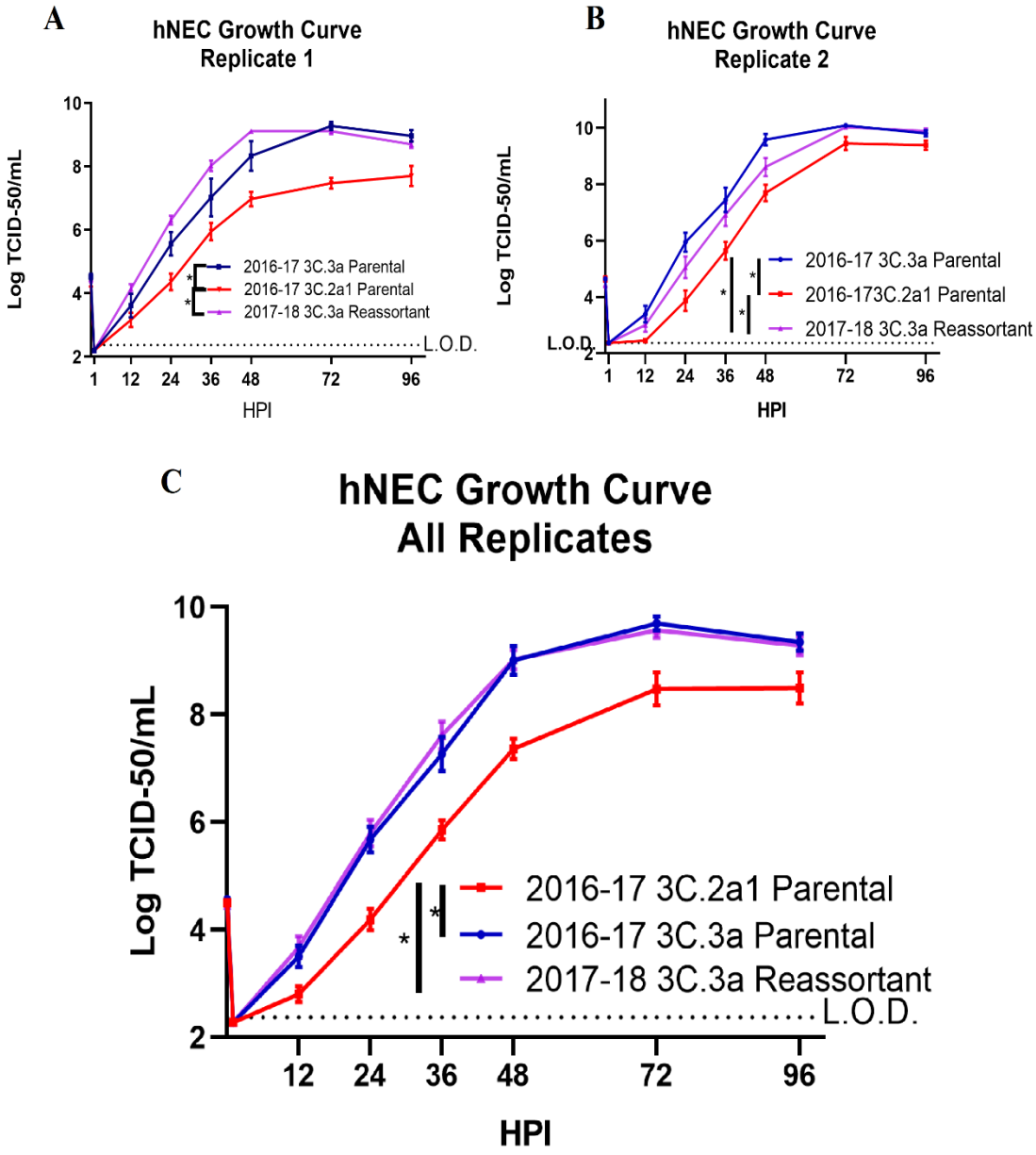

Figure 2.5

Two viruses from the three clades under study (2016-17 3C.2a1, 2016-17 3C.3a and 2017-18 3C.3a) were used to infect hNECs in low MOI (0.1) growth curves. Each individual growth curve (panels A and B) had four technical replicates for each virus. Panel C shows the data from both growth curves collapsed into a single graph.

Asterisks denote statistically significant differences ($p<0.05$) at two or more timepoints in a multiple-comparisons, two-way ANOVA between the clades indicated by the brackets. Error bars represent standard error of means (SEM).

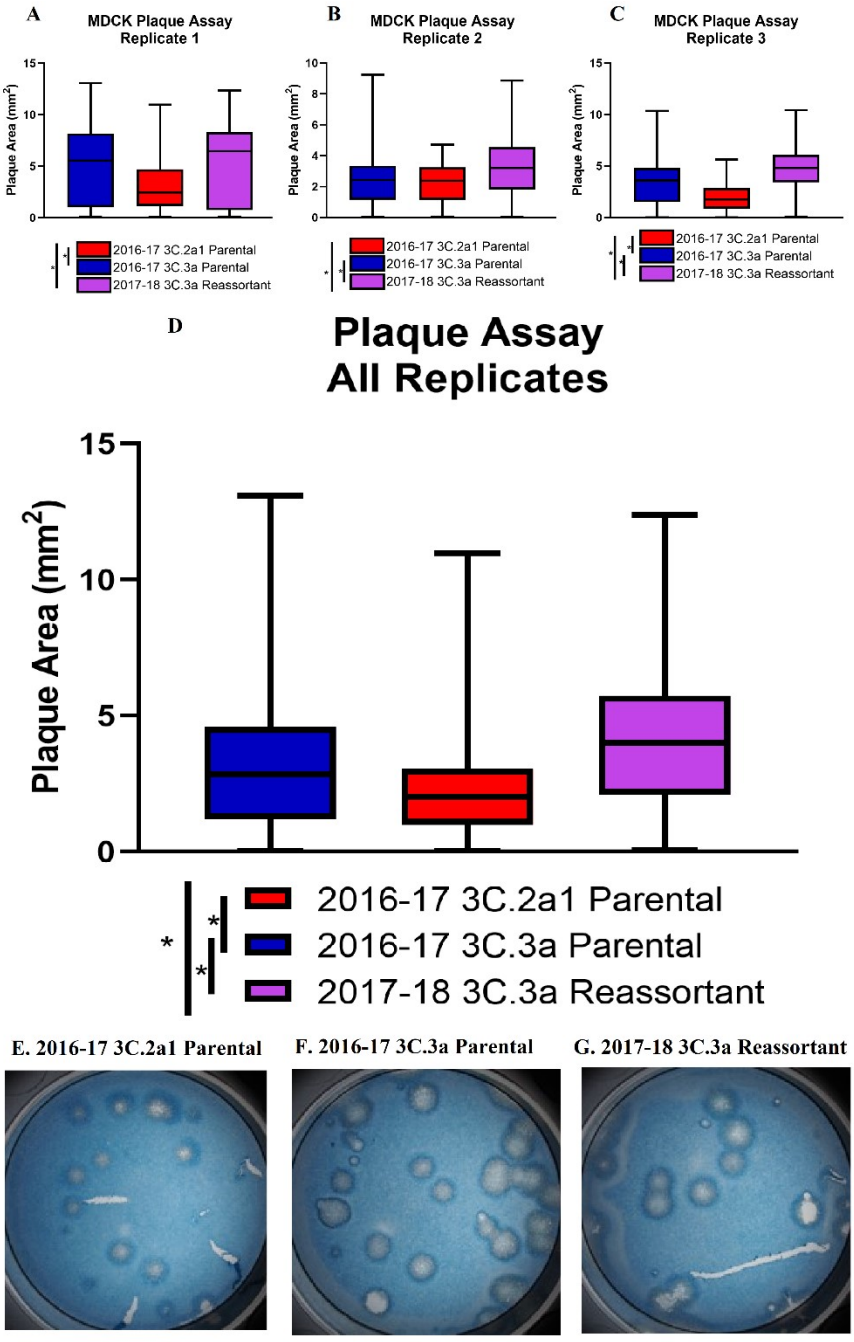

Figure 2.6
Two viruses from each clade under study were used to infect MDCK cells, and plaque area was quantified for each virus. Three biological replicates (panels A, B and C) were conducted with each virus having two technical replicates. Panel D shows data from all three biological replicates collapsed into a single figure. Asterisks denote statistically significant differences ($p<0.05$) via one-way ANOVA between clades.
Panels E, F and G are representative images of wells infected with a virus from each clade. Panel E represents the 2016-17 3C.2a1 parental clade, panel F the 2016-17 3C.3a parental clade and panel G the 2017-18 3C.3a reassortant clade.

Plaque Assay All Replicates Data Summary

Clade	Mean Plaque Area (mm^2)	Mean Difference: x - 2016-17 3C.2a1 Parental	Mean Difference: x - 2016-17 3C.3a Parental	Ratio: x:2016-17 3C.2a1 Parental	Ratio: x:2016-17 3C.3a Parental
2016-17 3C.2a1 Parental	2.242		-1.122		0.666
2016-17 3C.3a Parental	3.364	1.122		1.500	
2017-18 3C.3a Reassortant	4.160	1.918	0.796	1.855	1.237

Figure 2.7
These data were collected across all three biological replicates of the plaque assays. Column 1 lists the viral clades, and column 2 shows their associated mean plaque area in mm^2. Column 3 calculates the difference in plaque area means between each clade and the 2016-17 3C.2a1 parental clade, and column 4 does the same using 2016-17 3C.3a as the reference. Column 5 takes the ratio between each clade's mean plaque area and that of the 2016-17 3C.2a1 clade, while column 6 performs the same calculation using the 2016-17 3C.3a parental clade as the reference.

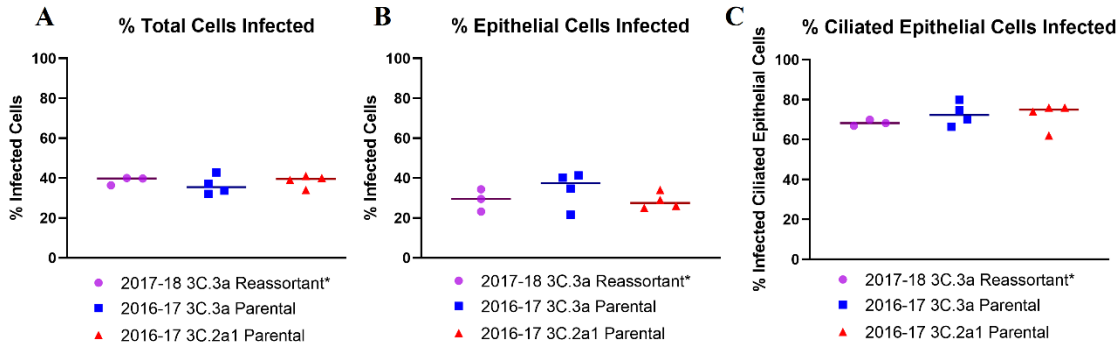

Figure 2.8
Panel A shows the percentage of cells exposed to human serum bound to goat-antihuman AF 647 antibodies, representative of infected cells relative to all cells present in the sample.
Panel B shows the percentage of cells exposed to human serum bound to Ep-CAM PE and goat-antihuman AF-647 antibodies, representative of infected epithelial cells relative to all epithelial cells present in the sample.
Panel C shows the percentage of cells exposed to human serum bound to Ep-CAM PE, goat-antihuman AF-647 and beta-tubulin, representative of nfected ciliated epithelial cells relative to all ciliated epithelial cells present in the sample.
The asterisk indicates that one 3C.3a replicate during the infection of hNECs prior to flow did not properly infect the cells, and the data have been excluded.

Chapter 3 – Determining Phenotypic Contributions of Reassorted Gene Segments

Experimental Rationale

The results obtained from the experiments described in Chapter 2 showed that reassorting 3C.3a gene segments HA, M and NS into an otherwise 3C.2a1 background conferred upon the progeny virus enhanced replication phenotypes relative to the parental 3C.2a1 viruses from 2016-17. Since the three gene segments from the 3C.3a background represented the largest difference between the 3C.3a reassortant and 3C.2a1 parental viruses, it seemed likely that one or more of these gene segments might be contributing to the enhanced replication phenotypes observed in both the $TCID_{50}$ and plaque assays.

To determine which gene segments were responsible, the phenotypic effects of each gene segment reassorted individually into a 3C.2a1 background on viral fitness would need to be examined. To begin, the gene segments for a 3C.2a1 parental virus would have to be cloned into a vector capable of producing infectious virus particles. pHH21 was chosen given its routine use in the Pekosz lab for cloning individual gene segments from IAVs. Each gene segment that had undergone reassortment (HA, M and NS) from a 3C.3a reassortant virus from the 2017-18 season into pHH21 would also need to be cloned into pHH21 to generate recombinant reassortant viruses.

Once all 3C.2a1 gene segments, along with 3C.3a HA, M and NS had been successfully cloned into pHH21, viruses would be rescued by transfecting 293T cells with these cloned plasmids and expression plasmids that code for influenza A polymerase proteins to assist in producing new virions. For control purposes, a recombined virus that contained all of the 3C.2a1 gene segments and another virus that contained all three 3C.3a reassortant gene segments in the 3C.2a1 background would be needed as they should recapitulate the phenotype of the clinically isolated 3C.3a reassortant and 3C.2a1 parental viruses. Each single reassortant 3C.3a gene segment (HA, M and NS) in a 3C.2a1 background would be needed to test the phenotypic impact

they confer individually, as measured through $TCID_{50}$ of supernatants obtained from an MDCK-Siat growth curve.

Materials and Methods

Cloning into pHH21

The plasmid selected for generation of infectious clones of the 3C.2a1 clinical isolate R0145 from 2016-17 was pHH21, diagrammed in figure 3.1. pHH21 contains sequences of DNA recognized by the restriction enzyme BsmBI which, upon enzymatic digestion, expose palindromic nucleotide sequences that can ligate with DNA digested by either BsmBI or another restriction enzyme, BsaI. These enzymatic cut sites are flanked by promoter and terminator DNA sequences for RNA polymerase I, which produces RNA without any 5' or 3' modifications, similar to that seen with influenza A virus genomic RNAs. The presence of an ampicillin resistance gene allows for transformation of bacterial cells and subsequent selection on ampicillin-impregnated LB agar plates of colonies derived from bacterial cells that had successfully been transformed with pHH21.

Common Cell Lines

For the amplification of pHH21 bearing 3C.2a1 and 3C.3a gene segments, the *Escherichia coli* DH5α cell line was used due to the ease with which it can be transformed with plasmids from the environment. Immortalized human kidney 293T cells were used to produce infectious influenza A virus via transfection. MDCK and MDCK-Siat cells (discussed at length in Chapter 2's materials and methods section) were applied as an overlay to 293T cells to amplify nascent recombinant viruses produced from cloned gene segments. Characterization of the generated recombinant viruses involved plaque assays conducted on MDCK cells and growth curves with subsequent $TCID_{50}$ assays conducted in MDCK-Siat cells, whose protocols have already been described in Chapter 2.

Cloning Influenza A Viral Gene Segments into pHH21

Two viruses were selected for cloning: 2016-17 Baltimore isolated influenza A H3N2 3C.2a1 R0145 and 2017-18 Baltimore isolated influenza A H3N2 3C.3a R0230. Figure 3.2 summarizes the gene segments cloned from each of these viruses and several characteristics of each gene segment, including length in kilo-basepairs, annealing temperatures and extension times used in PCR, the presence of enzymatic digestion sites for restriction enzymes BsaI and BsmBI within the open reading frame of the gene segments, and the expected fragment size via gel electrophoresis when digested by SalI and XmaI restriction enzymes.

Polymerase Chain Reaction

The first step in inserting viral gene segments into pHH21 was to perform polymerase chain reaction (PCR) using primers specific to each gene segment to amplify each gene segment individually. Reaction tubes were prepared by mixing together appropriate volumes of nuclease free water with 5x High-Fidelity PCR buffer, 5 μM forward and reverse primers specific for each gene segment (see figure 3.2), cDNA from the chosen virus (either R0145 or R0230), Phusion DNA polymerase and 10 mM dNTP. After vortexing and centrifuging reaction tubes, a thermal cycler with a PCR program containing the appropriate extension time and annealing temperature for the gene segments undergoing PCR (see figure 3.2) would be used to carry out the reaction.

Gel Electrophoresis

Once the gene segments had undergone PCR amplification, gel electrophoresis was performed to determine if the gene segment was of the correct expected base pair length by comparing to a ladder of known size (figure 3.3 shows the ladder used, while figure 3.2 shows the expected length of each gene segment). A 1% agarose gel solution was prepared by microwaving 1 gram of agarose in 100 mL of milli-Q purified water. Prior to casting, 10 μL of ethidium bromide was added to bind to the DNA and fluoresce under exposure to UV light. After casting,

the gel would be loaded into an electrophoresis case and covered in TAE buffer. Then, 10 µL of 5x loading dye would be added to the 50 µL PCR product, mixed thoroughly, and loaded into a well on the gel. Typically, gels would be run for one hour at 150 V or until the dye bands had visibly migrated approximately three-fourths of the distance from the well to the distal end of the gel. Exposing the gel to UV light and comparing the length of bands in the PCR products against the expected length of bands for each gene segment (figure 3.2) would reveal whether PCR had successfully cloned the gene segment. If so, the PCR products could be purified from the gel to continue processing.

Gel Extraction

Extraction from the 1% agarose gel was accomplished with a QIAquick Gel Extraction Kit, and the protocol followed was identical to the one provided (19). Extracted PCR products were eluted in 30 µL of nuclease free water and were ready to process through enzymatic digestion.

Enzymatic Digestion of pHH21 and/or gel-purified PCR products

In order to prepare the amplified gene segment for insertion into pHH21, enzymatic digestion of both the gene segments and pHH21 needed to be performed in order to generate exposed palindromic sequences that could be ligated. Figure 3.2 shows which gene segments would cut within the open reading frame of each gene segment (if a gene segment contains a BsmBI cut site inside its open reading frame, that segment would have to be digested via BsaI, and vice versa). pHH21 was always digested with BsmBI.

The reaction mixture consisted of nuclease free water, 10x Buffer 3.1, the gel extracted PCR products or pHH21, and the appropriate restriction enzyme. After mixing, vortexing and spinning down the reaction tubes, they would be incubated overnight at different temperatures depending on the enzyme contained within the reaction (55 C for BsmBI, 37 C for BsaI). The

following morning, the enzyme would be inactivated via incubation at their appropriate temperatures (80 C for BsmBI, 65 for BsaI) for 20 minutes.

When digesting pHH21, prior to inactivating enzymes, 0.5 μL of alkaline phosphatase would be added to the reaction mixture to prevent re-ligation of pHH21 to itself. After incubating at 37 C for one hour, the reaction would then undergo an inactivation incubation at 80 C for 20 minutes.

Purification of digested pHH21 and PCR products

After enzymatic digestion the digested DNA was purified away from the digestion reaction solution with a QIAquick PCR Purification Kit. The protocol used was identical to the one provided (21). Purified PCR products would be eluted in 30 μL, while pHH21 would be more highly concentrated at 20 μL. The concentration of each sample would then be measured on a NanoDrop spectrophotometer and recorded for calculations in the next step – ligation.

Ligation of pHH21 to purified gene segment digestions

A molar ratio of 1-part pHH21 to 3-parts gene segment insert was desired for optimal ligation. An online calculator was used to obtain the correct volumes needed of purified gene segment insert and pHH21 (17), and the appropriate volumes of pHH21 and gene insert were added to a clean thermal-cycler tube, along with nuclease free water, T4 DNA ligase, and 10x buffer specific for the ligase. In a separate tube, a no-insert control would be prepared as a negative control to guard against contamination. Once the reaction tubes had been mixed by pipetting and centrifuged, they would be incubated in a thermal cycler overnight at 16 C.

Transformation of DH5α Cells with pHH21+insert Plasmid

Following ligation, the gene-segment bearing pHH21 needed to be amplified. DH5α *E. coli* cells were used to achieve this. First, these bacterial cells would be removed from -80 C

storage and thawed on ice for 20 minutes, during which time a water bath would be prepared at 42 C. After thawing, 5 µL of the ligation reaction would be added to a tube containing 50 µL of bacterial cells and mixed by pipetting. This mixture would be incubated on ice for 30 minutes, after which the bacterial cells would be heat shocked in the 42 C water bath for 30 seconds, then immediately cooled on ice for two minutes. Sterile SOC or LB media would be mixed with the DH5α cells. Ampicillin-impregnated agar plates, after being warmed to room temperature, would be covered with DH5α cells using sterile glass beads. Once the beads had been removed, the plates would be incubated overnight at 37 C.

After transforming bacterial cells plates were checked for colony growth. If colonies were present on the pHH21 with gene segment inserted and absent on the no insert control plates, then colonies would be selected for growth in liquid culture.

Growing Liquid Cultures of DH5α cells & Miniprep

Culture tubes would be filled with 5 mL of liquid LB with dissolved ampicillin in preparation for DH5α cell inoculation. Using a sterile pipette tip, up to six colonies from each gene segment-bearing pHH21 plate would be selected and inoculated into the appropriate culture tubes, which would be incubated overnight in a shaking incubator at 37 C, 250 rpm. The following morning, tubes would be visually evaluated for bacterial growth, indicated by cloudiness in the media, and checked for contamination by foreign microbes. Assuming both DH5α cell growth and an absence of contamination, the liquid cultures could then be processed through a miniprep to isolate the amplified plasmid DNA. Additionally, 720 µL of liquid culture would be removed from the culture tubes and added to 180 µL of 80% glycerol solution and stored at -80 C for future use.

A QIAquick Plasmid Miniprep kit was used to purify plasmid DNA. The protocol followed was identical to the one provided in the kit (20). Purified plasmid DNA would be eluted

in 40 μL of nuclease free water. The concentration of the sample would then be obtained via NanoDrop spectrophotometer and recorded.

XmaI and SalI Digestion of pHH21 with ligated gene segments

Assuming a good quality and concentration of the miniprep purified plasmid products, the next step would be to subject the ligated pHH21 and insert to digestion with the restriction enzymes XmaI and SalI-a crucial preliminary step that determines whether the gene segment of interest had been successfully inserted into pHH21.

For this reaction, 500 ng of plasmid DNA was added to nuclease free water, 10x CutSmart buffer, and both XmaI and SalI restriction enzymes. Additionally, two control reactions were prepared: in the first, an empty pHH21 plasmid with no inserted gene segments would be loaded into a reaction tube with all components described above to determine what a no-insert sample would look like for comparison. The second control would be consist of a pHH21 sample with a ligated gene segment being placed into a reaction tube with no XmaI or SalI, to provide a no-enzyme comparison. Once all experimental and control tubes had been prepared, they would be loaded into a thermal cycler to incubate at 37 C overnight.

The following day, a 1% agarose gel would be prepared and run according to the protocol discussed previously. At the conclusion of the run, the gel would be examined to determine the length of the bands for each pHH21 and gene segment being verified If the band lengths present in gel electrophoresis match the expected band lengths in figure 3.2, then the sample will most likely contain the inserted gene segment corresponding to those band lengths. To verify this, the sample must be submitted to the Johns Hopkins School of Medicine sequencing facilities for sequence confirmation. The generated sequence can then be compared (using the Geneious sequencing software) to the known sequence for the corresponding gene segment. If there are no non-synonymous mutations within the open reading frame, then the plasmid with the insert may be expanded via ZymoPURE II MaxiPrep protocol to produce large quantities for rescue.

ZymoPURE II Maxiprep Expansion

From the glycerol stock solutions, an overnight culture of 150 mL in LB liquid media with ampicillin would be prepared. The following day, the ZymoPURE II Maxiprep kit would be used to isolate plasmid DNA from the bacterial culture. The protocol followed was identical to the centrifugation variant supplied in the kit (29). After eluting plasmid DNA in 400 μL of nuclease free water, the isolated plasmid should then be evaluated via NanoDrop spectrophotometer to determine concentration and purity.

Assuming no contamination, the products of MaxiPrep should then be submitted for sequencing to determine if any mutations occurred during the MaxiPrep process. If not, then the plasmid can be stored in -80 C until needed for producing infectious clones. Once all 3C.2a1 gene segments and the 3C.3a HA, M and NS gene segments have been successfully amplified via MaxiPrep it becomes possible to produce infectious clones of virus from the plasmids.

Generating Infectious Clones from Plasmids

Since viruses in the Pekosz lab are routinely grown in MDCK and MDCK-Siat cells, the first rescue experiments performed were meant to determine which cell type would be most conducive to rescuing these cloned viruses following transfection of 293T cells. These experiments sought to answer two questions: could the 3C.2a1 rR0145 plasmids produce infectious clones, and which cell type between MDCK and MDCK-Siat would allow for optimal viral rescue? Figure 3.4 diagrams the process of these initial experiments, while figure 3.5 summarizes the viruses sought from rescue.

To successfully rescue viruses from the cloned plasmids, viral polymerase protein-expressing plasmids from the H3N2 A/Udorn/1972 virus strain were used to supply the polymerase activity needed to generate mRNA from the transcribed genomic RNA produced from inserted viral gene segments. A strain of IAV isolated from a Victoria outbreak and cloned into pHH21, maintained by the lab and known to successfully be rescued at high titers, was used

as a positive control. Negative controls included mixtures of plasmids for 3C.2a1 rR0145 that included no HA or NA segments, Victoria virus without HA/NA, transfection reagent that contained no viral gene segments and OPTI-MEM that contained no transfection reagent.

Initial Rescue Experiments of 3C.2a1 rR0145

In a six-well plate, 500 µL of Poly-L-lysine must be added to each well and evenly distributed via rocking. Wells were then washed twice with PBS+. 293T cells could then be seeded into the wells at a concentration of between 2 and $3x10^5$ cells/well. After seeding, plates were incubated at 37 C for 24 hours. The following day, wells were checked by light microscopy to verify that 293T cells had attained between 40-60% confluence. If so, then transfection reagent TransIT-LT1 would be warmed to room temperature and vortexed. A master mix of consisting of OPTI-MEM and TransIT-LT1 could then be prepared. Aliquots of the master mix in Eppendorf tubes would then be mixed with the appropriate plasmids to generate the desired virus to be rescued (see figure 3.5), though for these initial experiments only the 3C.2a1 gene segments were used. After preparing the control reactions (Victoria all plasmids, Victoria lacking its HA and NA gene segments, 3C.2a1 lacking its HA and NA segments, no transfection reagent and cells only), media would be aspirated off of the 293T cells. Each well would then be washed with PBS+, after which 2 mL of OPTI-MEM would be added per well. The appropriate transfection reaction complex would then be added to each well, and the cells would be incubated at 32 C for 24 hours.

The next day, MDCK and MDCK-Siat cells were split and, following trypsinization, diluted to a concentration of $5x10^5$ cells per well. After achieving this concentration, the cells would then be spun down in a centrifuge and resuspended in infectious media. The OPTI-MEM media within the 293T cell wells would then be aspirated, and 2 mL of the MDCK or MDCK-Siat containing infectious media would be deposited into the 293T cell wells. The plates would then

be incubated at 32 C, and every 24 hours 1 mL of the supernatant would be collected for future use and replaced with 1 mL of freshly made infectious media per well.

During these rescue experiments, monitoring for cytopathic effects (CPE) helps gauge the success of each rescue, but subsequent verification of infectious virus presence is needed. This can be done via plaque assay of the rescue supernatants from each time point where CPE were observed. If CPE was not obvious in the wells, $TCID_{50}$ can be performed to determine whether virus is present in the supernatants, which can determine which supernatants would likely produce the best plaques in a subsequent plaque assay.

For the first rescue experiments, $TCID_{50}$ was performed on both MDCK and MDCK-Siat cells using the same protocols from chapter 2 (Figure 3.13). This was done to determine which cell type would be best for future titering experiments of rescued viral supernatants. Consistent with results from chapter 2, MDCK-Siat cells were better both for overlay of 293T cells and subsequent titering and, therefore, were used in future experiments for these purposes.

Generation of Seed Stocks

Once titering experiments confirmed the presence of viruses in the supernatant, plaque assays on MDCK cells were used to generate clonally pure samples of virus (as each plaque should derive from a single virus propagating through proximal cells). To remove a plaque for isolation of virus, a specially prepared filtered pipette with a broad opening in its tip would be used. Typically, plaques were picked three days after infection and the resulting agar plugs incubated in infectious media for between an hour and overnight at 4 C.

Following incubation, the infectious media bearing the agar plug would then be used to infect confluent MDCK-Siat cells in a six-well plate, with one well being used for each picked plaque. After washing the MDCK-Siat cells with PBS+ twice, 250 µL of the agar-plug bearing infectious media would be added to the appropriate MDCK-Siat well. The plates would then be incubated at 32 C for one hour, after which the viral media would be aspirated off of the wells

and replaced with 2 mL fresh infectious media. Following this, the plates would be placed back into the 32 C incubator and be monitored, daily, for the development of CPE. Once approximately 50% of the cells within a well showed signs of CPE, 500 µL aliquots could be collected and stored at -80 C until needed.

Extracting viral RNA

Verification of seed stock sequences was crucial to ensure that no mutations had been introduced. Segments HA, M and NS were of particular interest since they were reassorted between viruses of the 3C.2a1 and 3C.3a clades and were therefore the focus of sequencing efforts. To do this, first viral RNA had to be isolated from the seed stock samples. This was done using the Qiagen RNeasy Mini Kit, and the protocol followed was identical to the one supplied in the kit (22). After eluting the RNA into 50 µL of nuclease free water, the RNA was placed into -80 C until needed for RT-PCR.

Characterizing Rescued Viruses

To determine which gene segments were responsible for the faster replication phenotype observed in the 3C.3a reassortant viruses from the 2017-18 season compared with the 3C.2a1 viruses from the 2016-17 season, MDCK-Siat growth curves were performed. After collecting viruses at each time point, they were titered and the data compiled for analysis. The protocols for these experiments do not differ from those discussed in chapter 2.

Results

Cloning R0145 & R0230 Gene Segments into pHH21

Figure 3.6 shows a composite gel image of two separate XmaI and SalI digestion reactions. The gel on the left shows bands consistent with the expected band lengths following digestion of the M, NP, NS, PB1, HA and PA gene segments that I had processed from cDNA generated from clinically isolated 2016-17 3C.2a1 R0145 (see figure 3.2). The gel at the right shows XmaI and SalI digestions for the gene segments NA and PB2 from the same virus. Each digested gene segment produced bands consistent with expected gene segment lengths from earlier Geneious analysis, suggesting that initial PCRs and ligation reactions had successfully integrated the gene segments into the cloning vector pHH21. Further verification was later obtained from sequencing analysis of submitted samples, which confirmed that each gene segment had been cloned into pHH21 and could proceed with viral rescue of rR0145.

Some difficulties were encountered in cloning R0230 HA, M and NS into pHH21. M and NS were processed simultaneously in the beginning, producing the XmaI and SalI digestion gel seen in figure 3.7. While subsequent sequencing verification confirmed that NS had been successfully ligated into pHH21, the "M" segments visible in this image were contaminated during processing and were sequenced matched with NS. From there, the M segment cloning process was restarted. Furthermore, there were problems cloning HA into pHH21 – figure 3.8 shows an unsuccessful XmaI and SalI digestion of clonally selected pHH21 bearing HA, which should have three bands. After consulting members of the Pekosz laboratory for assistance in troubleshooting, they recommended adjusting annealing temperatures and extension times during PCR.

To optimize the PCR conditions, gradient PCR was performed for both R0230 HA and M. The initial gel (shown in figure 3.9) with both gradient PCR products shows the results – HA seemed to amplify best at 65 C, while M did not amplify as well at the tested temperatures. To obtain an optimal annealing temperature for the M segment, another gradient PCR for M at new

temperatures that were slightly lower than the initial range was conducted. This time, M amplified best around 65.4 C (figure 3.10). After reprocessing the samples from PCR to XmaI and SalI digestion using the new optimized conditions, HA bands (figure 3.11) and M bands (figure 3.12) consistent with predicted lengths were obtained. Subsequent sequencing verification confirmed the successful integration of each gene segment into pHH21 and the plasmids were stored for future use in viral rescue experiments.

Initial Rescue of rR0145

R0145 was cloned first into pHH21 first. In line with the pipeline outlined in figure 3.4, it was important to verify that these gene segments were capable of producing infectious virus following transfection and determine the best cell type for overlay with 293T cells and subsequent titering of rescued viruses. $TCID_{50}$ results for the transfection supernatants are shown in figure 3.13. In keeping with results from chapter 2, at low viral titers rR0145 could not easily infect MDCK cells, so much so that using MDCK cells as an overlay to 293T cells produced no measurable quantities of virus, even when titered on MDCK-Siat cells. Moving forward, MDCK-Siat cells were used for all rR0145 overlays and $TCID_{50}$s as those conditions gave maximum amounts of infectious virus from the rescue supernatants (Figure 3.13). Figure 3.14 shows the results of the negative controls lacking HA and NA in both Vic and rR0145, with no infectious viruses detected. The positive control virus, Vic, was successfully rescued from all overlay conditions and titered well on both MDCK and MDCK-Siat cells (figure 3.15), suggesting that the difficulties encountered in rescuing rR0145 from MDCK cells were due to the virus, not deficiencies in the cell line.

Rescue of rR0145 with R0230 gene segments

After confirming the viability of the rR0145 gene segments to produce infectious virus, R0230 HA, M and NS had been cloned into pHH21 and required testing to determine whether

these gene segments, in combination with R0145's background, could successfully be rescued. To that end, I five plasmid mixes were prepared for transfection (summarized in the legend of figure 3.16). As a positive control, 293T cells were transfected with all eight gene segments of R0145 since that virus had been successfully rescued in a previous experiment (figure 3.13). One transfection consisted of all three R0230 cloned segments (HA, M and NS) combined with all other gene segments of R0145 to generate a virus that should be phenotypically similar to R0230. The three other transfections included only a single gene segment from R0230 in an R0145 background (monoreassortant viruses) to test which gene segment (or segments) recapitulated the R0230 phenotype. The results of $TCID_{50}$ of the viral supernatants in figure 3.16 show the successful rescue of rR0145 with all plasmids from the R0145 background, as well as rR0145 with R0230 HA, M and NS individually. The triple reassortant (rR0145 with R0230 HA, M and NS in the same virus) was not successfully rescued in this first experiment. A plaque assay of the rescued viruses was performed and seed stocks made.

A second viral rescue experiment was performed to obtain the triple reassortant rR0145 with R0230 HA, M and NS. Subsequent $TCID_{50}$ quantification verified that the triple had been rescued (figure 3.17). This experiment involved three conditions seeking to rescue the triple reassortant virus: one where the concentrations of 3C.3a segment-bearing plasmid were the same as the previous experiment, one in which they were doubled, and one in which both the 3C.3a and Udorn plasmid concentrations were doubled. Figure 3.17 shows that the original plasmid concentration condition was the only triple-reassortant condition to yield any infectious viruses. While it was unusual that the rescue of rR0145, all plasmids, failed to produce any detectable clearance of cells in the $TCID_{50}$, a plaque assay was performed to isolate clonally pure virus and subsequently generate seed stocks.

Generating Seed Stocks of rR0145 and rR0145 with R0230 Segments

The goal of this plaque assay was to generate clonally pure viral samples for future characterization. Distinct plaques should result from a single virus propagating through adjacent cells, and therefore should be identical to the progenitor virus responsible for infecting the first cell at the center of the plaque (barring any mutations). After picking distinct plaques via micropipette tip and transferring them to infectious media, these isolated plaques were used to infect freshly plated MDCK-Siat cells. Once approximately fifty percent of MDCK-Siat cells exhibited CPE, 500 µL aliquots were collected and stored at -80 C. The initial plaque assay saw rR0145 all plasmids and the single reassortant rR0145 with either R0230 HA, M or NS all produce clonally distinct plaques, which were picked and grown for the production of seed stocks. The second plaque assay, conducted with rR0145 containing all three R0230 segments HA, M and NS, was also successful and plaque picking produced monoclonal isolates of the triple reassortant virus.

$TCID_{50}$ of Seed Stocks of rR0145 and rR0145 with R0230 Segments

The seed stocks were titered in order to prepare working stocks and an MDCK-Siat growth curve at an initial MOI of 0.001. The results of this $TCID_{50}$ analysis of the rescued viral seed stocks are presented in figure 3.18. Using these viral titers, a growth curve on MDCK-Siat cells was conducted using a rescued 3C.2a1 virus with all 2016-17 parental 3C.2a1 gene segments (rR0145), 3C.2a1 viruses including either the 3C.3a HA, M or NS gene segment in place of the 3C.2a1 gene segment, and clinically isolated 2016-17 3C.2a1 (R0145) and 2017-18 3C.3a (R0230) viruses. The results of $TCID_{50}$ analysis of this growth curve are shown in figure 3.19. Consistent with work from chapter 2, the reassortant 3C.3a virus, R0230, replicated to higher viral titers at earlier timepoints than the parental 3C.2a1 virus, R0145. Among the rescued viruses, rR0145 with 3C.3a HA replicated at earlier timepoints to higher titers than all other rescued viruses and the parental, clinically isolated 3C.2a1 virus.

Discussion

Figures 3.6, 3.11 and 3.12 show that all 3C.2a1 gene segments, as well as 3C.3a HA, M and NS, were successfully cloned into a pHH21 cloning vector for the eventual generation of rescued recombinant viruses. While troubleshooting was extensive for these plasmids, all segments were sequence verified and subjected to Maxiprep amplification for use in rescue.

Viral rescue experiments to isolate the necessary combinations of R0145 and R0230 gene segments proved successful, though only if 293T cells were overlaid with MDCK-Siat cells (Figure 3.13). This is consistent with findings from chapter 2 that repeatedly showed that MDCK cells could only successfully be infected by the 2016-17 3C.2a1, 3C.3a and 2017-18 3C.3a viruses at relatively high MOIs (greater than 0.001 typically used for low MOI growth curves). Fortunately, since the desired viruses could be recovered from MDCK-Siat overlaid rescue experiments, we were able to proceed with characterization of the effects of each individual gene segment reassortment from the 2017-18 3C.3a reassortant virus, R0230, into the 2016-17 3C.2a1 parental virus R0145.

Since clinically isolated viruses produced the same phenotype in both MDCK-Siats and hNECs (see chapter 2), the recombinant reassortant viruses from rescue seed stocks could be characterized on the lower-maintenance MDCK-Siat cell line. Figure 3.19 shows that, among the rescued recombinant viruses, the 3C.2a1 virus bearing the 3C.3a HA gene segment grew to the highest viral titers at the earliest timepoints. This suggests that the reassortment of 3C.3a HA into a 3C.2a1 background is enough to induce a significant increase in viral fitness. Because this is only an initial experiment with a single replicate, further study would be needed to confirm that 3C.3a HA consistently leads to an increase in fitness when reassorted into a 3C.2a1 background. Furthermore, because inclusion of 3C.3a HA alone in an otherwise 3C.2a1 background was not enough to completely recapitulate the reassortant phenotype, this strongly indicates that the NS and M gene segments are partially responsible.

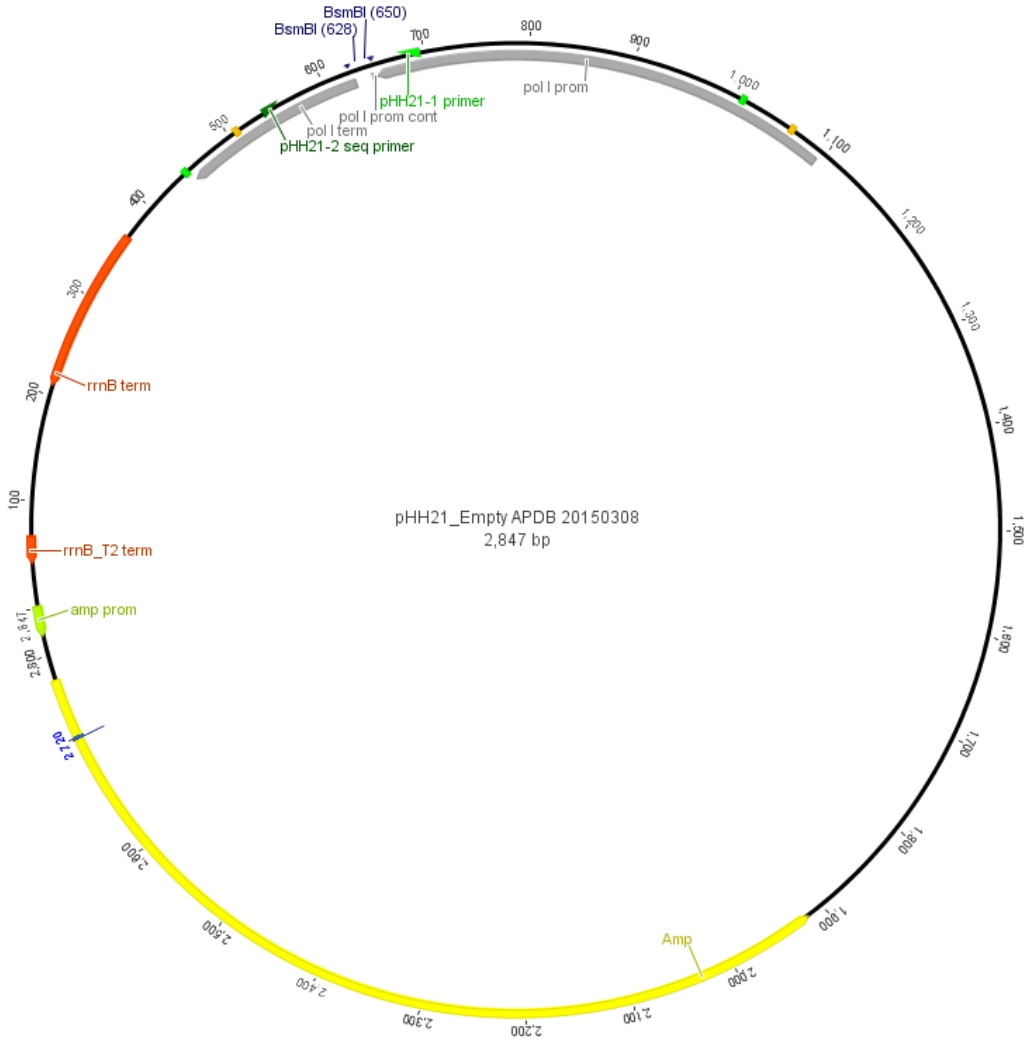

Figure 3.1
Diagram of the plasmid vector used for cloning, pHH21. Of note are the BsmBI cut sites (in navy), the ampicillin resistance gene (in yellow), and the pHH21 primer binding sites (in green). Image was developed using Geneious software.

Virus	Gene Segment	Length	Primer Set	Annealing Temperature	Extension Time	BsaI/BsmBI Digestion site?	XmaI/SalI Digestion Fragments(bp)
2016-17 H3N2 3C.2a1 Baltimore R0145	HA	1.7 kb	FluA3, FluA4	65 C	1 min	BsmBI	2601, 1133, 632
2016-17 H3N2 3C.2a1 Baltimore R0145	NA	1.5 kb	FluA15, FluA16	55 C	1 min 30 sec	BsaI	2601, 1026
2016-17 H3N2 3C.2a1 Baltimore R0145	PB1	2.4 kb	FluA11, FluA12	65.9 C	1 min 30 sec	BsmBI	2601, 1587, 757
2016-17 H3N2 3C.2a1 Baltimore R0145	PB2	2.4 kb	FluA13, FluA14	62 C	1 min 30 sec	Both BsmBI and BsaI	2601, 2417
2016-17 H3N2 3C.2a1 Baltimore R0145	PA	2.3 kb	FluA9, FluA10	68.4 C	1 min 30 sec	BsaI	2601, 2232
2016-17 H3N2 3C.2a1 Baltimore R0145	NP	1.5 kb	FluA7, FluA8	66.8 C	1 min 10 sec	BsmBI	2601, 1566
2016-17 H3N2 3C.2a1 Baltimore R0145	M	1 kb	FluA1, FluA2	68.4 C	35 sec	BsmBI	2601, 1026
2016-17 H3N2 3C.2a1 Baltimore R0145	NS	0.9 kb	FluA5, FluA6	68.4 C	35 sec	BsmBI	2601, 889
2017-18 H3N2 3C.3a Baltimore R0230	HA	1.7 kb	FluA3, FluA4	65 C	1 min	BsmBI	2601, 1133, 632
2017-18 H3N2 3C.3a Baltimore R0230	M	1 kb	FluA1, FluA2	65.4 C	35 sec	BsmBI	2601, 1026
2017-18 H3N2 3C.3a Baltimore R0230	NS	0.9 kb	FluA7, FluA8	68.4 C	35 sec	BsmBI	2601, 889

Figure 3.2
This table shows the viruses (column 1) and gene segments from each virus (column 2) selected for cloning into pHH21. Length of each gene segment is given in kilobasepairs in column 3. Primer set used to amplify each gene segment is provided in column four. The annealing temperature and extension time used in PCR are supplied in columns five and six respectively. Column seven whether each gene segment contains digestion sites for BsaI and/or BsmBI within their open reading frames. Column eight shows the expected fragment sizes, in basepairs, generated when each gene segment ligated into pHH21 is digested by restriction enzymes XmaI and SalI.

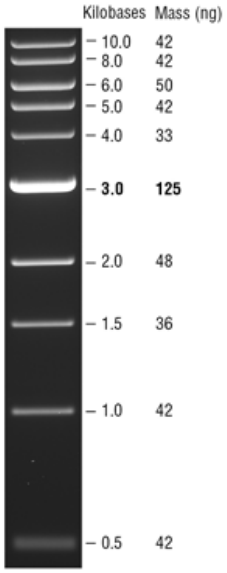

Figure 3.3
1 kb ladder used during gel electrophoresis for comparing experimentally generated fragments of nucleic acid to bands of known length (34).

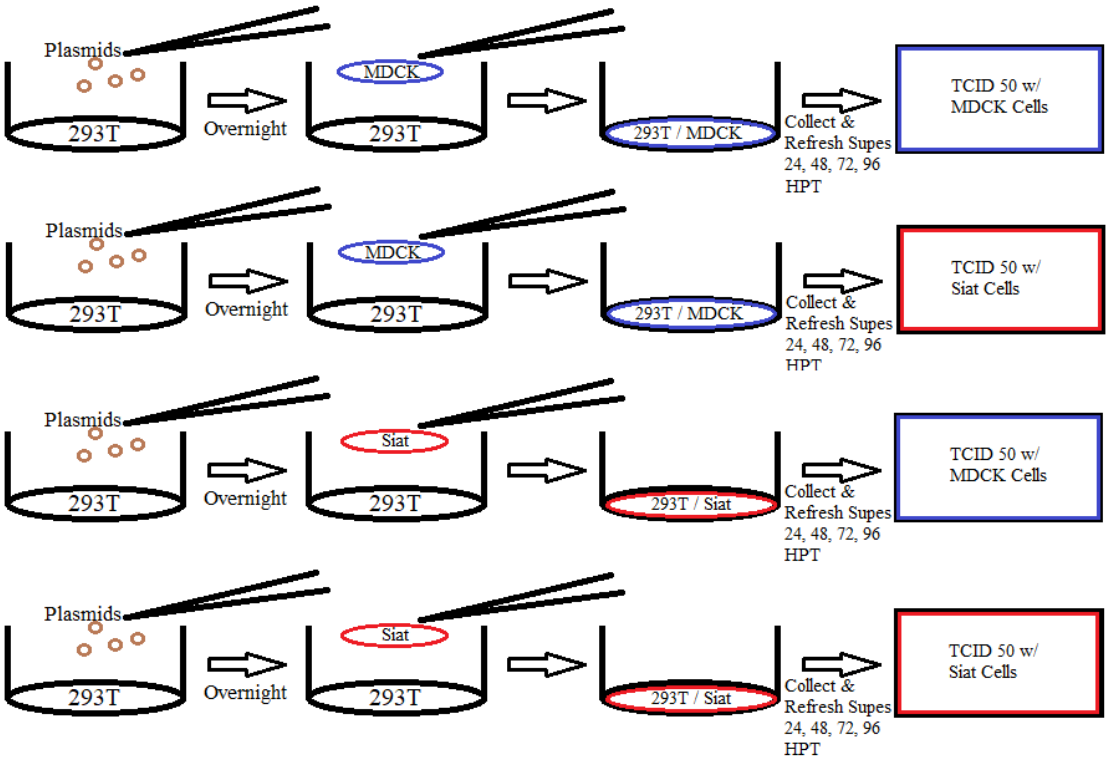

Figure 3.4
This diagram shows the experimental procedures conducted to generate and confirm the presences of rescued viruses and to determine which cell type was better for future experiments. First, pHH21 plasmids ligated to gene segments would be incubated with 293T cells overnight. Then, either MDCK (blue) or MDCK-Siat (red) cells would be added as an overlay to allow nascent viral particles to amplify. After collecting supernatant samples from the 293T cells overlaid with either MDCK or MDCK-Siat cells, titering would be performed on either MDCK or MDCK-Siat cells.

Viruses Sought from Rescue	Gene Segment Clade of Origin in Rescued Virus							
Sample ID	HA	M	NS	NP	PA	PB1	PB2	NA
rR0145	3C.2a1	3C.2a1	3C.2a1	3C.2a1	3C.2a1	3C.2a1	3C.2a1	3C.2a1
rR0145 w/ R0230 HA, M, NS	3C.3a	3C.3a	3C.3a	3C.2a1	3C.2a1	3C.2a1	3C.2a1	3C.2a1
rR0145 w/ R0230 HA	3C.3a	3C.2a1	3C.2a1	3C.2a1	3C.2a1	3C.2a1	3C.2a1	3C.2a1
rR0145 w/ R0230 M	3C.2a1	3C.3a	3C.2a1	3C.2a1	3C.2a1	3C.2a1	3C.2a1	3C.2a1
rR0145 w/ R0230 NS	3C.2a1	3C.2a1	3C.3a	3C.2a1	3C.2a1	3C.2a1	3C.2a1	3C.2a1

Figure 3.5
This table shows the viruses sought from rescue. Sample IDs identify which gene segments are meant to be contained within each virus, with red boxes indicating a gene segment arose from the 3C.2a1 virus isolated during the 2016-17 outbreak, Baltimore R0145, and purple boxes that the segment originated from the 3C.3a virus isolated in the 2017-18 flu season, Baltimore R0230.

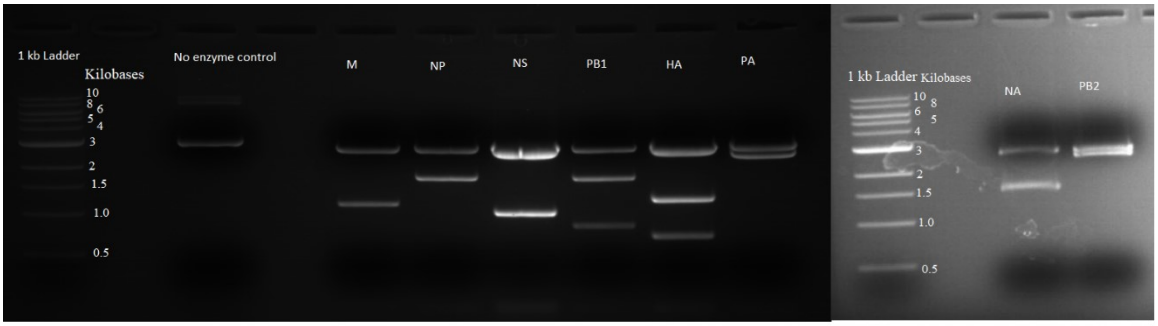

Figure 3.6
This composite gel image shows gene segments from 2016-17 H3N2 3C.2a1 Baltimore R0145 digested by the XmaI and SalI restriction enzymes, with ladders and a no restriction enzyme control displayed at far left. Each gene segment was compared to the expected lengths from figure 3.2 and matched them. These segments were submitted for sequencing verification.

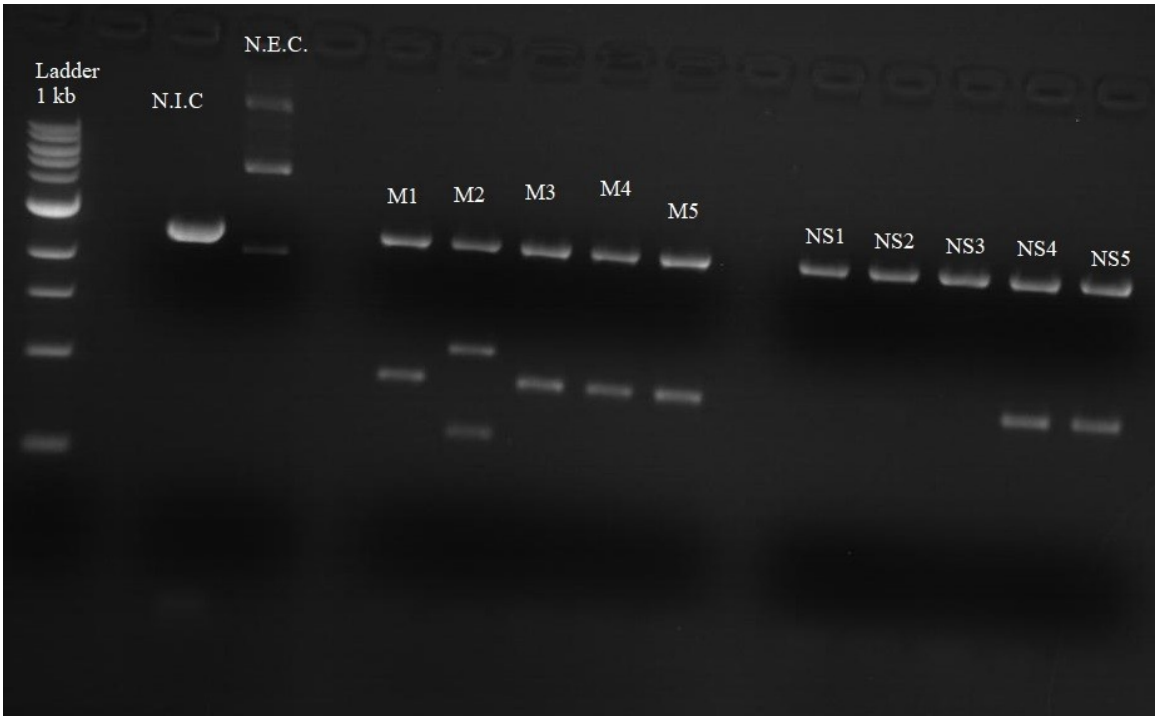

Figure 3.7
This gel shows the XmaI and SalI digestion of the M and NS segments of 2017-18 H3N2 3C.3a Baltimore R0230. Samples M1, M3, M4 and M5, along with samples NS4 and NS5 were submitted for sequencing. The M samples submitted for sequencing were found to be contaminated with NS segment DNA, while the NS4 and NS5 samples submitted were pure.

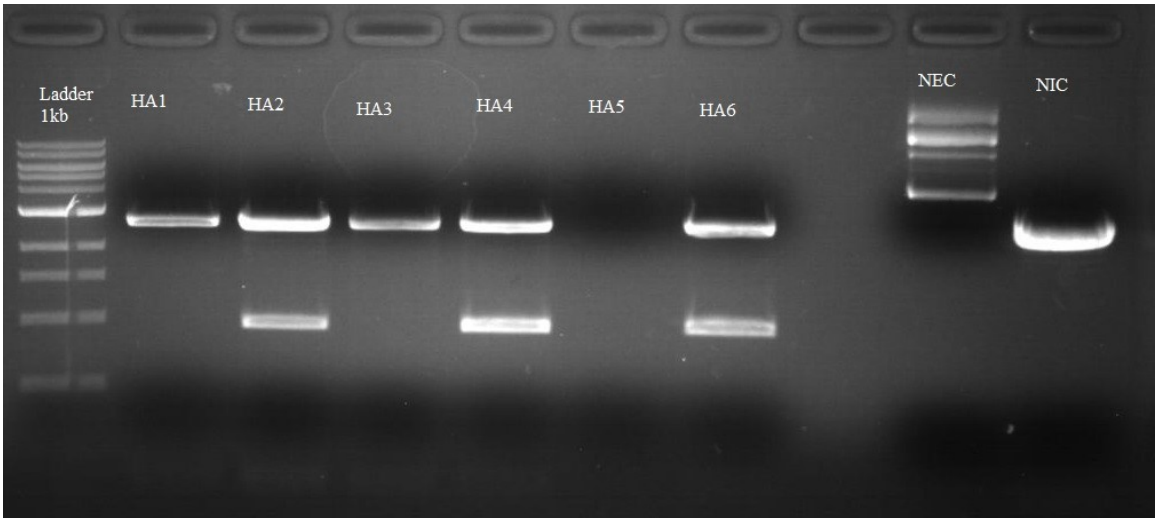

Figure 3.8
This gel shows 2017-18 H3N2 3C.3a Baltimore R0230's HA segment after XmaI and SalI digestion. None of the samples showed the expected band lengths described in figure 3.2.

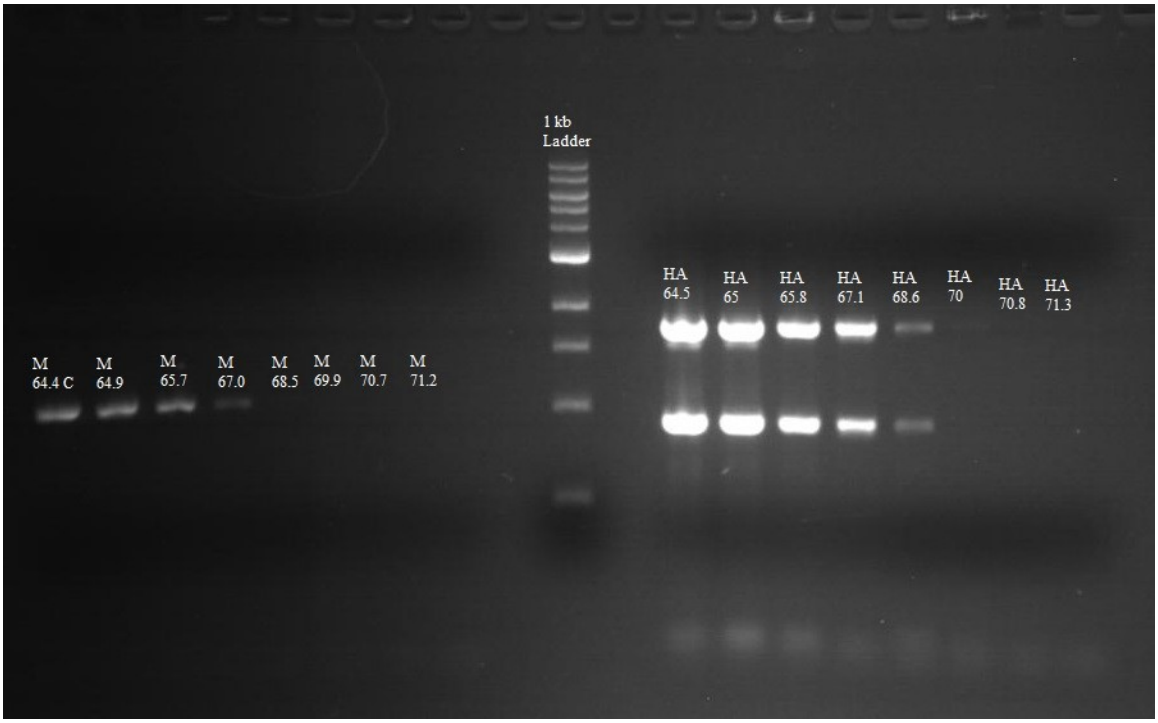

Figure 3.9
This gel shows the results of an annealing temperature gradient PCR experiment on 2017-18 H3N2 3C.3a Baltimore R0230's M and HA segments to determine the ideal annealing temperature for each reaction. For HA, 65 C was selected for future experiments. None of the M segment bands matched the intensity of the HA bands, and so a second gradient PCR experiment was necessary to identify the ideal annealing temperature.

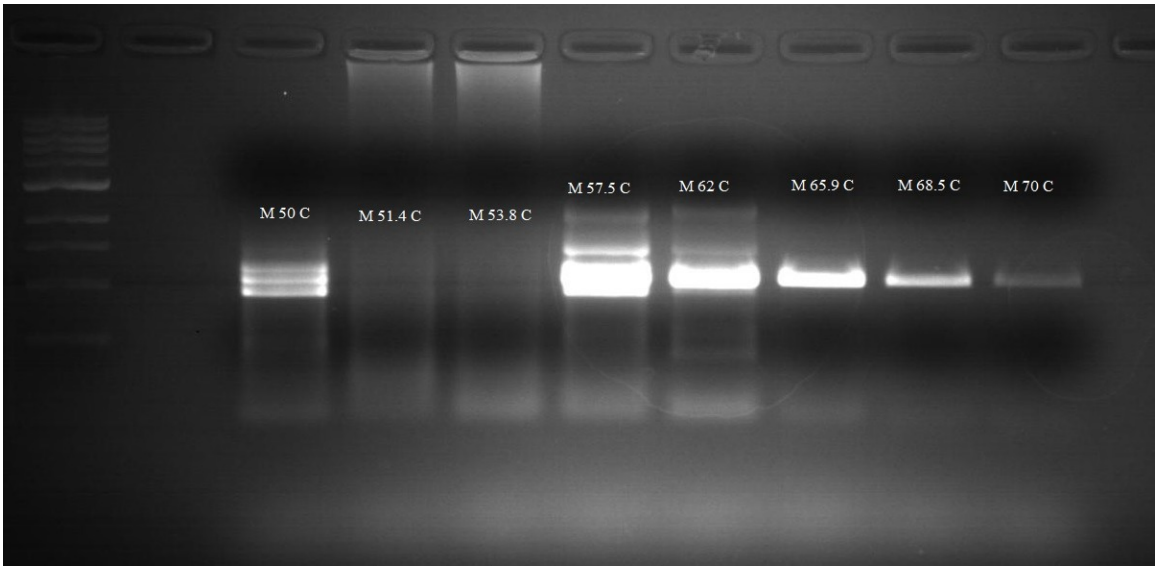

Figure 3.10
This gel shows the results of the second annealing temperature gradient PCR experiment conducted on 2017-18 H3N2 3C.3a Baltimore R0230's M segment. The intensity of the band generated at 65.9 C, coupled with a lack of degraded bands, made this the temperature used for future PCR experiments.

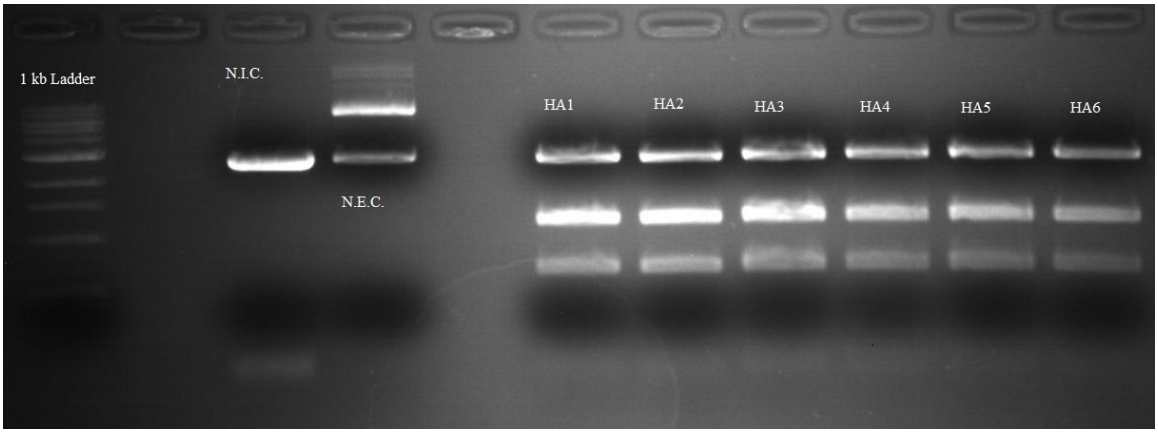

Figure 3.11
This gel shows the HA segment of 2017-18 H3N2 3C.3a Baltimore R0230 after XmaI and SalI digestion following PCR with the new annealing temperature derived from annealing temperature gradient PCR in figure 3.9. Each sample contained the expected band lengths from figure 3.2.

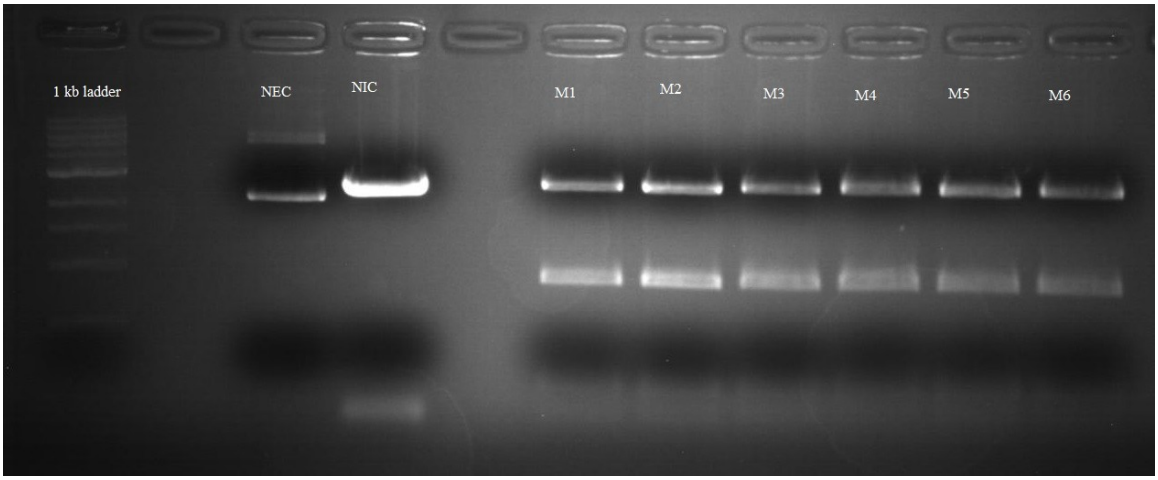

Figure 3.12
This gel shows the HA segment of 2017-18 H3N2 3C.3a Baltimore R0230 after XmaI and SalI digestion following PCR with the new annealing temperature derived from annealing temperature gradient PCR in figure 3.9. Each sample contained the expected band lengths from figure 3.2.

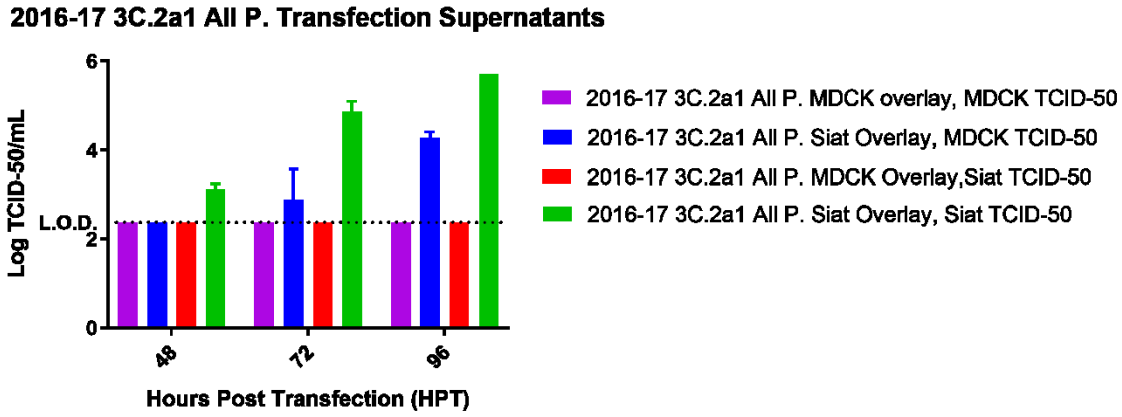

Figure 3.13
This graph shows the $TCID_{50}$ results following the initial rescue experiments conducted with both MDCK and MDCK-Siat overlays on 293T cells. Results from titering on both MDCK cells and MDCK-Siat cells are shown. The purple bars represent data from titering experiments conducted with MDCK overlay on 293T cells, and titered on MDCK cells. Blue represents an MDCK-Siat overlay whose supernatants were then titered on MDCK cells. Red shows data from supernatants collected from an MDCK overlay that were then titered on MDCK-Siat cells. Green displays data taken from supernatants collected from an MDCK-Siat overlay that were subsequently titered on MDCK-Siat cells. The only conditions that showed successful virus generation were the conditions where MDCK-Siat cells were used to overlay 293T cells (green and blue), and the best titering data came from MDCK-Siat cells (green). For all future rescue experiments, 293T cells would be overlaid with MDCK-Siat cells and titering of supernatants would be conducted on MDCK-Siat cells.

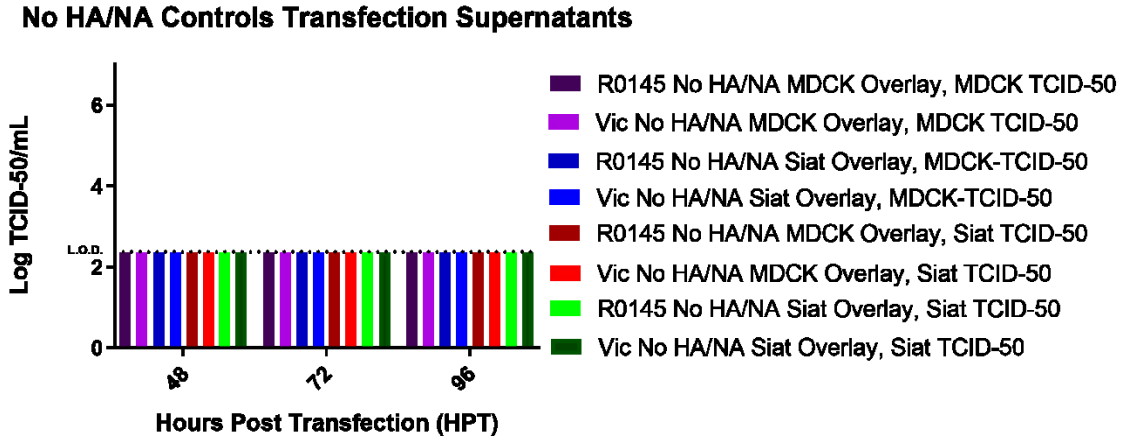

Figure 3.14
Each bar in this graph represents a negative control reaction where both the positive control virus, Vic, and the desired virus rR0145 lacked HA and NA in the initial rescue experiments. As expected, no titers were detected, regardless of MDCK or MDCK-Siat cell overlay on 293T cells or whether MDCK or MDCK-Siat cells were used for titering.

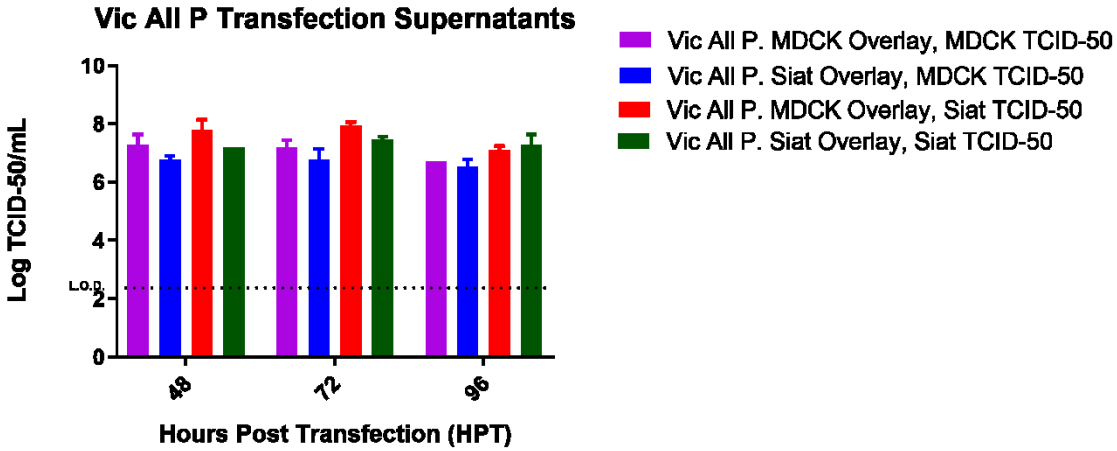

Figure 3.15

This graph shows the titering results from the positive control virus in the initial viral rescue experiment. Consistent with previous results in the Pekosz lab, the virus was successfully rescued from both MDCK and MDCK-Siat overlays on 293T cells and could be titered equally well on both MDCK and MDCK-Siat cells.

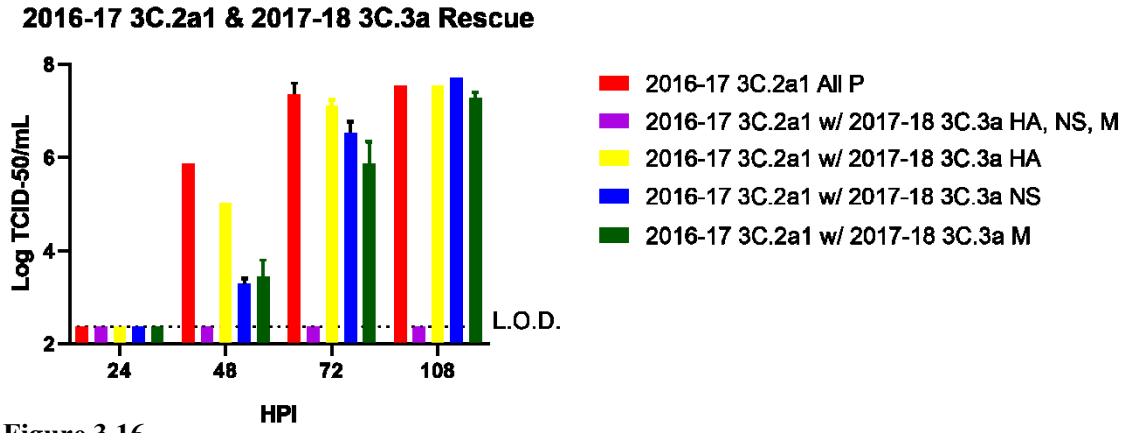

Figure 3.16

This graph shows titering conducted of rescued viruses containing all gene segments from 2016-17 H3N2 3C.2a1 Baltimore R0145 (red) or with gene segments from 2017-18 H3N2 3C.3a Baltimore R0230 replacing a single 3C.2a1 gene segment (HA in yellow, NS in blue, and M in green). The triple reassortant 3C.2a1, supposed to contain 3C.3a HA, M and NS, was not rescued in this experiment.

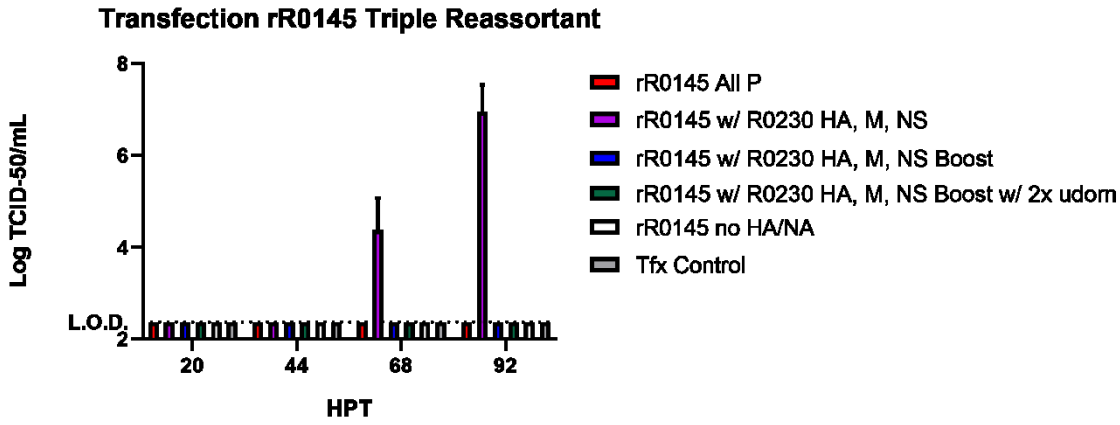

Figure 3.17
These titering data show the successful rescue of a recombinant 2016-17 H3N2 3C.2a1 Baltimore R0145 containing HA, M and NS from 2017-18 H3N2 3C.3a Baltimore R0230 following a troubleshooting experiment. Boosting the concentration of 3C.3a HA, M and NS plasmids in the absence (blue) or presence of doubled udorn expression plasmid concentrations (green) resulted in no infectious virus being generated, though standard concentrations of the 3C.3a HA, M and NS plasmids (purple) did produce infectious virus..

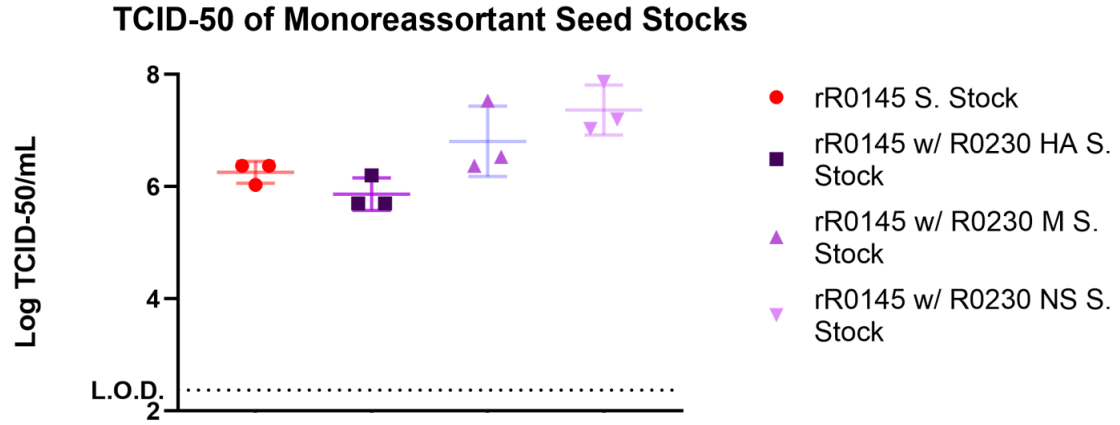

Figure 3.18
These are titers of seedstocks of the rescued 3C.2a1 virus, rR0145, and each of the monoreassortant viruses (rR0145 with either HA, M or NS from 3C.3a R0230) that were used for future experiments.

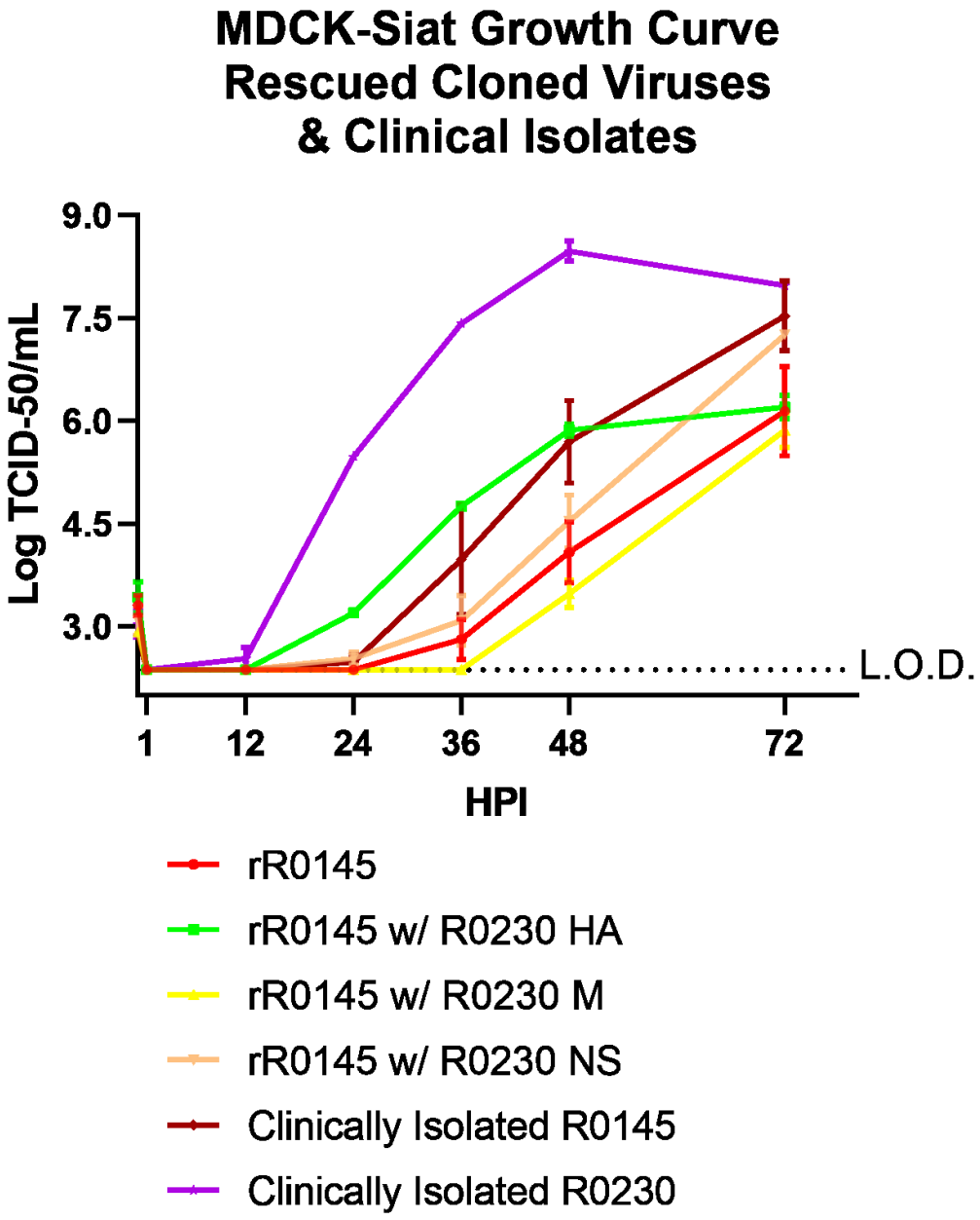

Figure 3.19
This MDCK-Siat growth curve titering data shows each of the rescued viruses (3C.2a1 rR0145 with all 3C.2a1 plasmids, the monoreassortant rR0145 rescues with either 3C.3a HA, M and NS) as well as two clinically isolated viruses, 2017-18 H3N2 3C.3a reassortant Baltimore R0230 and 2016-17 H3N2 3C.2a1 Baltimore R0145, grown simultaneously. The purple graph, representing the clinically isolated reassortant 3C.3a, again replicated earlier to higher viral titers than the parental 3C.2a1 in crimson, consistent with results from chapter 2. Of the rescued viruses, rR0145 with R0230 HA (green) most closely recapitulated the phenotype of the reassortant 3C.3a virus, growing to higher titers at earlier timepoints than all viruses (including the parental 3C.2a1 virus) except the actual reassortant R0230 virus. Error bars here represent standard error of means.

Reassortment's Association with Enhanced Viral Fitness

Growth curve experiments conducted on MDCK-Siat (figures 2.3-2.7) and hNECs (2.8-2.10) demonstrated that reassortant 3C.3a viruses isolated in the 2017-18 US influenza season replicated to higher viral titers at earlier time points than parental 3C.2a1 viruses isolated in the 2016-17 season. If enhanced viral replication in these cell lines, especially hNECs, can be used as a proxy for *in vivo* transmissibility and virulence, then these results are consistent with the greater number of outpatient visits in the 2017-18 season resulting from influenza-like illness than during the 2016-17 season (8). Therefore, the initial hypothesis – that reassortment of gene segments from the 3C.3a clade into a 3C.2a1 background could lead to increased viral fitness, thereby explaining some of the difference in the severity noted between the 2016-17 and 2017-18 flu seasons (3) – is consistent with results obtained from experimental analysis of viral growth rates when compared to the relative severity of the two flu seasons under study. However, the reassortant 3C.3a virus had similar replication kinetics as the 3C.3a parental virus, so reassortment did not improve the fitness when compared to that parental virus.

When trying to determine the relative effect that the 3C.3a reassortment might have had on the severity of the 2017-18 flu season, it is important to consider the relative number of cases of influenza resulted from 3C.3a infections. Had 3C.3a experienced a surge in case numbers during the 2017-18 season and become the dominant circulating viral clade of H3N2, that would offer very strong evidence that the 3C.3a reassortment event played a large role in the increased severity of the 2017-18 season over that of 2016-17. The situation was not so simple, as can be seen in figure 4.1 (9). Among specimens collected from influenza-positive patients across the United States by public health laboratories and reported to the CDC, 3C.3a viruses accounted for only 1% of all H3N2 cases in the 2017-18 outbreak, while 3C.2a viruses (including 3C.2a2 but excluding 3C.2a1) were reported in 84% of influenza cases (5). In Baltimore, specimens collected as part of the CEIRS network found 3C.3a viruses representing a larger portion of the

influenza cases reported (19%), though 3C.2a2 viruses still accounted for substantially more cases (41%). Since 3C.2a2 was more abundant in the United States during the 2017-18 outbreak (8), both nationally and within the CEIRS samples collected in Baltimore, perhaps the 3C.2a2 viruses were more responsible for the increase in virulence noted in that season. To more fully grasp the effect of reassortment on H3N2 viral fitness, and the potential impacts thereof on inter-seasonal differences in case-load and severity of influenza in the U.S., a discussion on 3C.2a2's reassortment event is necessary.

While this research focused on the 3C.3a reassortment of HA, M and NS into a 3C.2a1 background, the 3C.2a2 reassortment event of HA and PB1 into the 3C.2a1 background was also investigated. The same sorts of growth curves and $TCID_{50}$ assays as used in this thesis were conducted to study these viruses, and the findings mirror those reported here. In MDCK-Siat cells, the 2017-18 and 2016-17 3C.2a2 viruses grew to higher titers at earlier timepoints than the 3C.2a1 viruses isolated in the 2016-17 season (figure 4.3, manuscript in progress). Reassortant 3C.2a2 viruses isolated from the 2017-18 outbreak also showed a small but consistent replication advantage over 3C.2a2 parental viruses from the 2016-17 season. Similar results were noted in his hNEC growth curves (figure 4.4, manuscript in progress). This suggested that the 3C.2a2 reassortment, like its 3C.3a counterpart, had conferred upon the reassortant 3C.2a2 viruses greater fitness than was present in the 2016-17 3C.2a1 parental viruses, despite sharing six gene segments with them.

Both reassortant 3C.3a and 3C.2a2 viruses evinced enhanced viral fitness compared to a previously dominant circulating clade, 3C.2a1. These reassortments, taken together, offer a compelling case for why the 2017-18 flu season was substantially more severe (8) than the 2016-17 outbreak. These reassortment events permitted reassortant viruses to replicate more rapidly to higher titers in hNECs than their parental 3C.2a1 viruses. Since 3C.2a2 viruses especially made up the majority of H3N2 cases of influenza during the 2017-18 outbreak, the dominant clade of

that season, this increased replication fitness could explain why more people became infected with and suffered more severe symptoms from influenza than during the 2016-17 season.

Vaccine Effectiveness in the 2016-17 and 2017-18 US Flu Seasons

Vaccination against H3N2 in both the 2016-17 and 2017-18 seasons in the United States was achieved using a virus derived from the H3N2 3C.2a Hong Kong strain. Now that findings have been presented demonstrating that the reassortment of 3C.3a HA, M and NS gene segments into an otherwise 3C.2a1 background likely increases the replication rate of the reassortant virus, it is important to examine how these changes might have impacted the protective effects of the H3N2 vaccine deployed in the 2017-18 U.S. flu season.

First, it will be helpful to examine both the 2016-17 and 2017-18 flu seasons' vaccine effectiveness. The vaccine deployed in 2016-17 had an overall vaccine effectiveness against all influenza A and B strains of 40%, while specifically against IAV H3N2 it was only 33% effective (2). The overall effectiveness of the 2017-18 vaccine against influenza A and B strains was a comparable 38%, but against IAV H3N2 the effectiveness was only 22% among all age groups – a one-third decrease in effectiveness compared to the previous flu season (2). Indeed, examining the age stratified effectiveness table for the 2017-18 season reveals that, for every group older than eight years, the 95% confidence interval of effectiveness included the null value of 0% (2). From a statistical perspective, vaccination for these groups was little better than not receiving a vaccine in terms of preventing illness from IAV H3N2. This was not the case for the 2016-17 vaccine – while people in the 18-49 and 65 and older age groups had 0% effectiveness within their 95% confidence intervals, every other age group statistically received a protective benefit receiving the vaccine (2).

The reassortment events that generated novel 3C.2a2 and 3C.3a viruses in the 2017-18 US flu season can help explain this decrease in vaccine effectiveness. Since the H3N2 component in both seasons' vaccines was derived from the same 3C.2a Hong Kong virus, the

new reassortant viruses might have been able to escape protective antibodies associated with vaccination since no new antibodies would be on hand to protect against the novel HA epitopes present on the reassortant 3C.2a2 or 3C.3a viruses. Indeed, as figure 4.6 shows, in 3C.3a viruses isolated during the 2017-18 season there were 14 amino acid changes compared to 3C.2a1 viruses that had circulated in 2016-17, with 11 of these occurring in the highly antigenic HA head domain. Given the relatively low vaccine effectiveness of 33% in the 2016-17 season, we must assume that the dominant 3C.2a1 viruses of that year and the 3C.2a Hong Kong derived vaccine virus likely had numerous amino acid differences in their HA head regions, which would only be increased by the 14 differences between 2017-18 reassortant 3C.3a and 2016-17 3C.2a1 viruses. However, attention must be paid to the fact that when the vaccines were being evaluated for protective benefits by the CDC, they found the 3C.2a1 and 3C.2a2 viruses circulating to be antigenically similar to the vaccine selected (2). One possible phenomenon to explain this discrepancy is that the viruses circulating in the 2017-18 outbreak were still antigenically recognized by antibodies produced by the immune system, but their replication kinetics allowed them to infect a new host, replicate to contagious titers and be transmitted to the next host before the antibodies could effectively control the infection. Further study would be needed to determine if this was indeed the case.

One hypothesis that this research did not explore is that the 3C.2a Hong Kong vaccine was partially protective during the 2016-17 outbreak, producing non-sterilizing immunity in recipients via cross-reactive antibodies capable of slowing, but not stopping, viral replication. However, this cross-reactivity might have been lost due to amino acid residue changes in the 3C.3a (and, presumably, the 3C.2a2) HA head domain resulting from reassortment before the 2017-18 season. If true, this lack of cross-reactive protection could help explain the increase in transmissibility and severity noted between the 2016-17 and 2017-18 US flu seasons.

3C.3a Cases on the Ascendance

This lack of protection might also explain another interesting phenomenon – the proportion of cases of H3N2 influenza resulting from 3C.3a viruses is on the rise. Thus far the 2018-19 flu season has been an H1N1 dominant year in the United States, accounting for over 50% of cases reported by public health laboratories resulting to the CDC, shown in figure 4.7 (5). However, 3C.3a now makes up 65% of all H3N2-caused cases of influenza in the United States, a 65-fold increase in the percentage of cases from the 2017-18 outbreak (or, looking at the raw numbers of cases, up from 11 3C.3a cases reported by public health labs to the CDC in 2017-18 to 383 in 2018-19, a nearly 35-fold increase).

This is not surprising: for the two consecutive flu seasons prior to 2018-19, the WHO had recommended the same H3N2 component, a 3C.2a virus, be used for the vaccine. Therefore, 3C.2a viruses would likely have been under extreme selective pressure to adapt to the robust immune response generated in vaccinated individuals. 3C.3a viruses would likely have faced less selective pressure, thereby alleviating them of the need to escape protective antibodies generated by previous years' vaccines. Furthermore, prior to the 2018-19 US flu season, the WHO recommended that a new H3N2 component be included in the flu vaccine, derived from a 3C.2a1 Singapore strain isolated in 2016 (33). This could explain why the proportion of 3C.2a1 and 3C.2a2 derived influenza cases in the US were lower than 3C.3a cases (figure 4.7). 3C.3a viruses likely would not have encountered robust antibody mediated immunity during the 2018-19 outbreak. Indeed, in all three outbreaks, there was no 3C.3a component of the influenza vaccine available in the U.S., which might explain the surge in cases resulting from 3C.3a viruses during the 2018-19 season (5).

This substantial increase in the proportion of U.S. influenza cases resulting from 3C.3a viruses did not escape the attention of the World Health Organization. Normally, they release their influenza vaccine recommendations in February to provide manufacturers sufficient time to prepare stocks. However, in evaluating the progress of the 2018-19 flu season within the United

States, the WHO elected to wait until March 21, 2019 to issue its recommendation, in which they advised that the H3N2 component of the vaccine be derived from a 3C.3a virus (24). This likely resulted from their concern about the potential for 3C.3a to become the dominant circulating clade in the 2019-2020 influenza season, at least in the United States. It will be interesting to see what effect this change in vaccine strain has, if any, on the proportion of influenza cases resulting from H3N2 3C.3a viruses in future outbreaks.

Future Directions

Most of the work in this thesis centered on the effects of mutations accrued in 3C.3a viruses because of the reassortment event. However, as figure 4.5 shows, there were some differences between 2017-18 3C.3a and 2016-17 3C.2a1 viruses that resulted from genetic drift. NA in particular showed the greatest number of such drift mutations. It would be interesting to generate a cloned, reassorted virus with 2017-18 3C.3a NA inserted in the 2016-17 3C.2a1 background and then perform growth curves and $TCID_{50}$s to characterize any phenotypic differences resulting from the NA drift mutations. Similar work could be done on the PB1 and PB2 segments, though each of these had fewer amino acid differences between the 3C.3a and 3C.2a1 isolates than NA.

The experiments conducted for this thesis were only able to determine phenotypic differences in replication in hNECs and immortalized MDCK-Siat and MDCK cells. In hNECs, which undergo a human innate immune response to infection, it would be interesting to characterize what effects various intra- and extracellular defenses were having against the 2017-18 3C.3a and 2016-17 3C.2a1 viruses. Any differential protection could explain why 3C.3a viruses were capable of replicating more rapidly to higher titers than 2016-17 3C.2a1 viruses. Cytokines, chemokines, and other immune molecules could be detected via ELISA and, if present on the surface of cells, flow cytometry. Any differences between cells infected with the different viruses could be captured and studied further.

As the 2018-19 US flu season winds down, JHU CEIRS has likely stockpiled new clinically isolated viruses for analysis. Since 3C.3a viruses were the dominant H3N2 circulating this past season clinical isolates from Baltimore would likely reflect this trend. One potential continuation of this work would begin with sequencing the newly isolated 3C.3a viruses and comparing them to the 2017-18 isolates. Given that this influenza season was mild compared to the 2017-18 season, with fewer cases reported to outpatient facilities at its peak (5), there was likely not another reassortment event that contributed substantially to an increase in 3C.3a viral fitness. Therefore, it seems likely that any mutations would have arisen through genetic drift between this year's 3C.3a viruses and last year's. Sequence comparisons could test these ideas.

Building upon the genetic analysis, future experiments to assess the fitness of 2018-19 3C.3a viruses, especially compared to 3C.3a viruses from previous flu seasons and 3C.2a viruses from the 2018-19 season, would be interesting. Comparing the phenotypes of 3C.2a2 and 3C.3a viruses isolated in the 2018-19 season with their 2017-18 counterparts would be interesting for several reasons. First, since 3C.2a2 viruses were far more common in the more severe 2017-18 outbreak than 3C.3a viruses (Figure 4.1), it might be worth examining 2018-19 3C.2a2 viruses to see if they exhibited similar phenotypes to those circulating in 2017-18. If the 3C.2a2 reassortment event was one of the key drivers of the severity of the 2017-18 season, then the milder 2018-19 season might be the result of mutations attenuating the 3C.2a2 phenotype, which could allow 3C.3a viruses to become dominant if their phenotype remained comparable between the 2018-19 and 2017-18 seasons. This hypothesis could be tested with hNEC growth curves and subsequent $TCID_{50}$s to compare replication phenotypes between viral clades isolated in each flu season. Another, similar, hypothesis is that 3C.3a viruses saw an increase in viral fitness compared to 3C.2a2 viruses and, therefore, were able to outcompete them. The same experiments discussed above could be used to test this hypothesis.

However, the relative surge of 3C.3a cases might not be due to a true fitness advantage over 3C.2a2 viruses – it might just be that the vaccine available today better protects against

3C.2a2 viruses, and therefore there simply are not as many cases of influenza presenting to JHU CEIRS resulting from infection with 3C.2a2 viruses. To test that hypothesis, the affinity of antibodies in human serum from the 2018-19 season against both circulating 3C.2a2 and 3C.3a viruses could be examined via antibody neutralizing titration assays, which would identify the concentrations of serum needed to neutralize the activity of the 3C.3a and 3C.2a2 viruses. These experiments might show that antibodies present in the population during the 2018-19 outbreak exhibit greater affinity for 3C.2a2 viruses since there are fewer cases of influenza resulting from 3C.2a2 infection this outbreak season (figure 4.7), especially given that the H3N2 component of the vaccine was a 3C.2a1 virus.

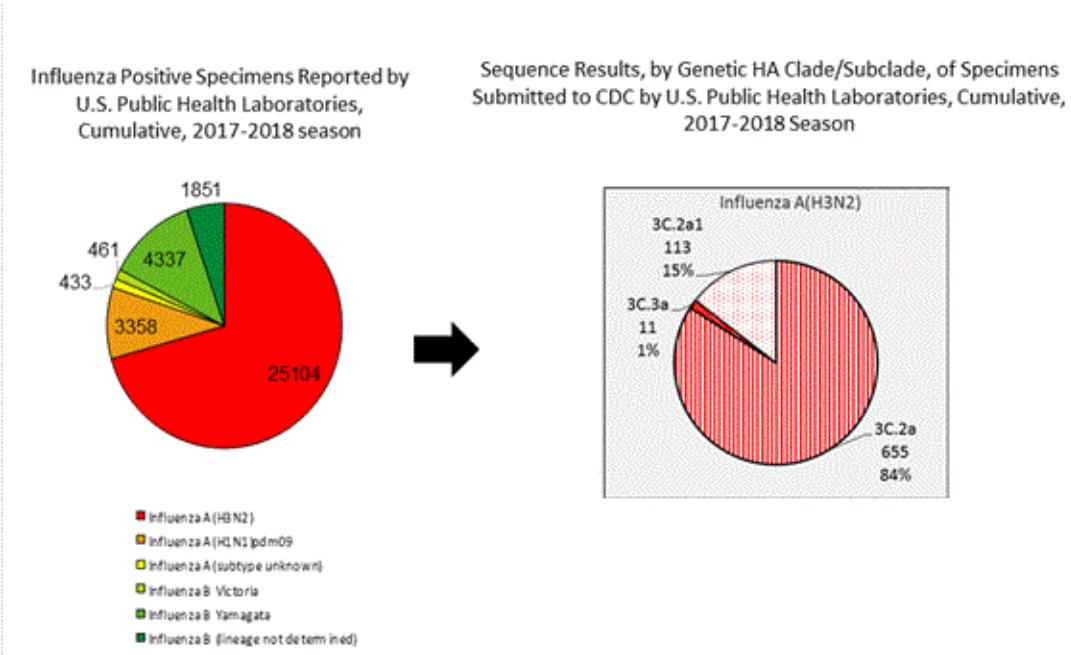

Figure 4.1
Panel A shows the cases reported to CDC caused by each subtype of influenza A and B in the 2017-18 season. IAV H3N2 accounted for most of the cases, and panel B breaks down the cases of H3N2 due to clades 3C.2a (including 2a2), 3C.2a1 and 3C.3a. (9)

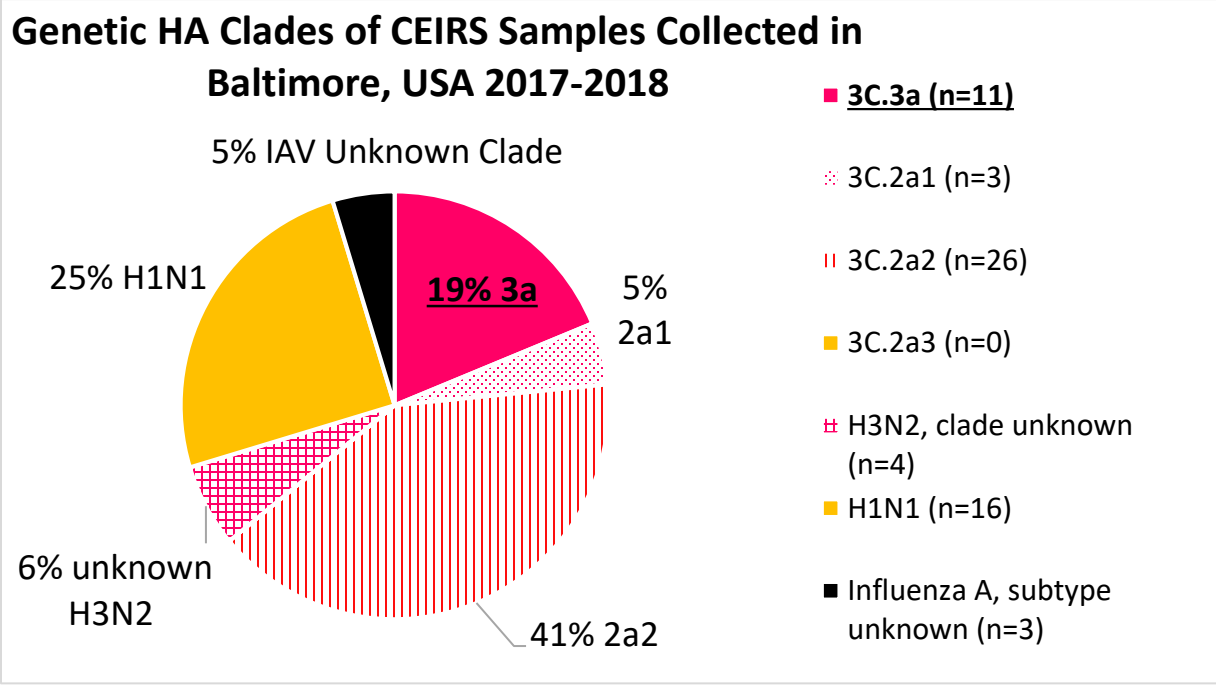

Figure 4.2
This pie chart shows IAV subtype and clade of samples submitted to JH CEIRS from Baltimore during the 2017-18 U.S. influenza season.

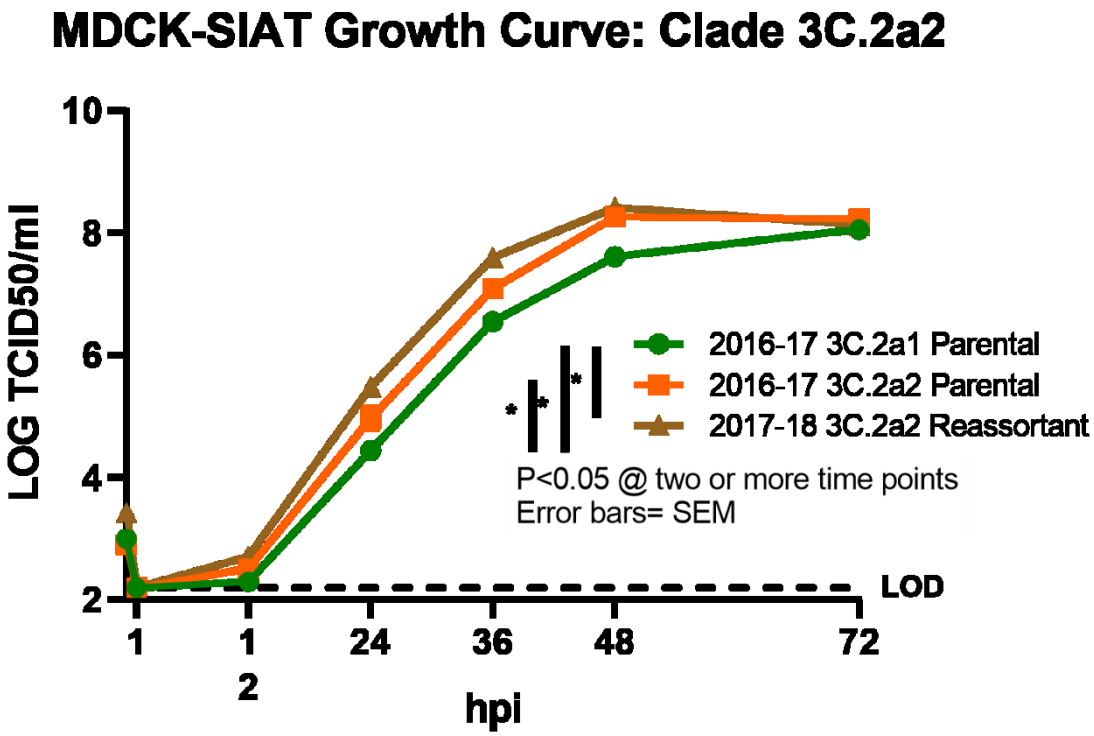

Figure 4.3
These data show three independent biological replicates, collapsed across clades, of MDCK-Siat growth curves conducted with 3C.2a1 (green) and 3C.2a2 (orange) parental viruses from the 2016-17 U.S. influenza outbreak, and 3C.2a2 reassortant viruses from the 2017-18 season (brown). The 3C.2a2 reassortant viruses grew at earlier timepoints to higher viral titers than either parental strain. Each virus was grown in quadruplicate (manuscript in progress).

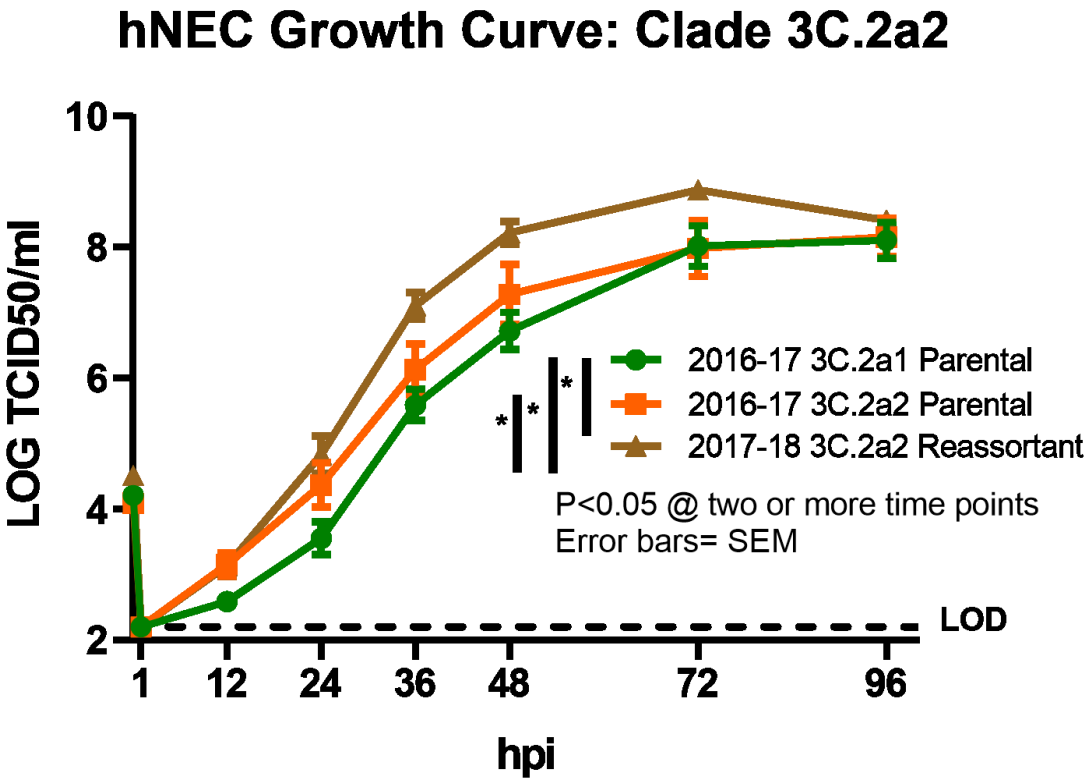

Figure 4.4
These data show three independent biological replicates of hNEC growth curves, collapsed across clades, conducted with 3C.2a1 (green) and 3C.2a2 (orange) parental viruses from the 2016-17 U.S. influenza outbreak, and 3C.2a2 reassortant viruses from the 2017-18 season (brown). The 3C.2a2 reassortant viruses grew at earlier timepoints to higher viral titers than either parental strain.
Each virus was grown in quadruplicate (manuscript in progress).

	Protein Open Reading Frames										
# of amino acid differences between 2017-18 3C.3a and…	HA	M1	M2	NS1	NS2	NA	NP	PB1-F1	PB1-F2	PB2	PA
H3N2 2016-17 Parental 3C.3a	1	0	0	0	0	13	1	4	3	1	0
H3N2 2016-17 Parental 3C.2a1	14	0	1	4	0	5	0	1	1	1	0
Amino acids per protein	566	252	97	231	112	469	498	760	92	759	716
% different: 3a reassortant vs 3a parental	0.18%	0.00%	0.00%	0.00%	0.00%	2.77%	0.20%	0.53%	3.26%	0.13%	0.00%
% different: 3a reassortant vs 2a1 parental	2.47%	0.00%	1.03%	1.73%	0.00%	1.07%	0.00%	0.13%	1.09%	0.13%	0.00%

Figure 4.5
This table summarizes sequencing analysis conducted on the gene segments of two viruses from each clade studied in this thesis (2016-17 3C.2a1 and 3C.3a parental, and 2017-18 3C.3a reassortant). Each gene segment was compared to a consensus sequence from the 3C.3a reassortant viruses, and the number of amino acid differences between each parental clade and the reassortant clade are reported here, as well as the % differences.

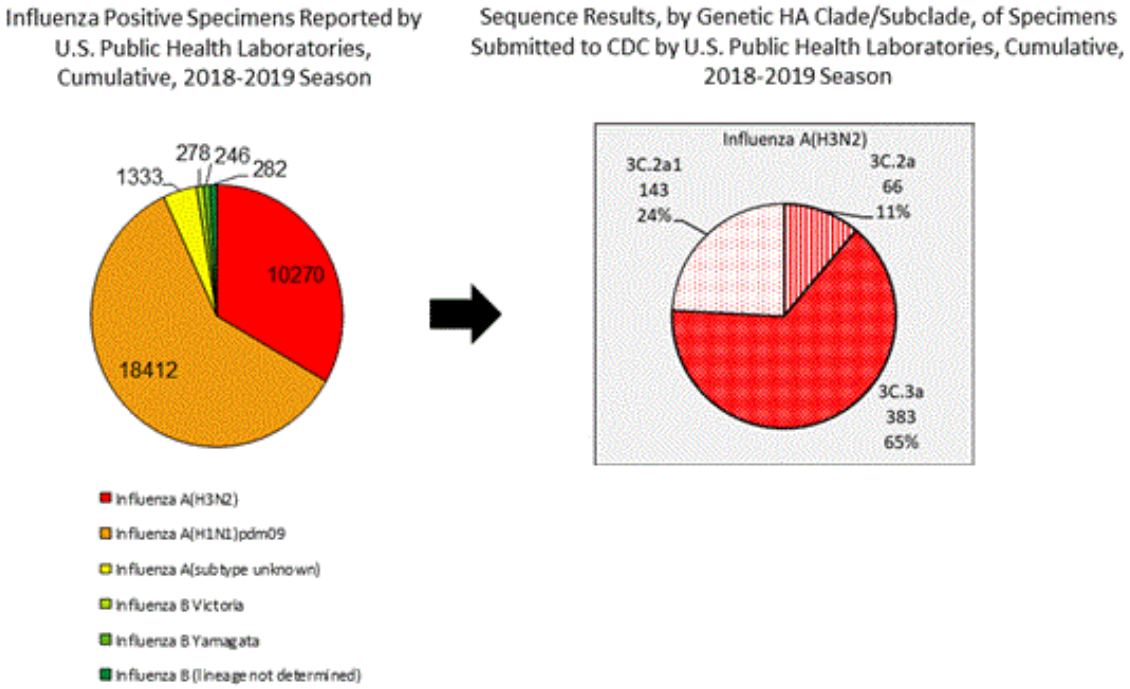

Figure 4.6
Panel A shows the cases reported to CDC caused by each subtype of influenza A and B in the 2018-19 season. IAV H1N1 accounted for most of the cases, though H3N2 was still reported in approximately 40% of cases. Panel B breaks down the cases of H3N2 due to clades 3C.2a (including 2a2), 3C.2a1 and 3C.3a. (5)

Bibliography

1. Centers for Disease Control and Prevention. (2018). Summary of the 2016-2017 Influenza Season. Retrieved from https://www.cdc.gov/flu/about/season/flu-season-2016-2017.htm
2. Centers for Disease Control and Prevention. (2018). Influenza (Flu) Seasonal Influenza Vaccine Effectiveness, 2017-2018 Tables, 2017–2018.
3. Centers for Disease Control and Prevention. (n.d.). Influenza-associated hospitalizations by virus type, 2016-17 & 2017-18 seasons. Retrieved November 2, 2019, from https://gis.cdc.gov/grasp/fluview/FluHospChars.html
4. Centers for Disease Control and Prevention. (2017). 2016-2017 Influenza Season Week 39 ending September 30, 2017. Retrieved from https://www.cdc.gov/flu/weekly/weeklyarchives2016-2017/Week39.htm
5. Centers for Disease Control and Prevention. (2019). 2018-2019 Influenza season week 5 ending February 2, 2019. Retrieved from https://www.cdc.gov/flu/weekly/index.htm
6. Centers for Disease Control and Prevention. (2017). Influenza (Flu) Seasonal Influenza Vaccine Effectiveness , 2016-2017 Tables, (1), 2016–2017.
7. Centers for Disease Control and Prevention. (2018). How Influenza (Flu) Vaccines Are Made. Retrieved from https://www.cdc.gov/flu/protect/vaccine/how-fluvaccine-made.htm
8. Centers for Disease Control and Prevention. (2018). 2017-2018 Influenza Season Week 39 ending September 29, 2018. Retrieved from https://www.cdc.gov/flu/weekly/weeklyarchives2017-2018/Week39.htm
9. Centers for Disease Control and Prevention. (2018). Summary of the 2017-2018 Influenza Season. *Centers for Disease Control and Prevention*, *11*, 7–10. Retrieved from https://www.cdc.gov/flu/about/season/flu-season-2017-2018.htm
10. Drake, J. W. (1993). Rates of spontaneous mutation among RNA viruses, *90*(May), 4171–4175.
11. Farmer, S., & Schaller, C. (2017). Cell-Surface carbohydrates and influenza viruses. In *LibreTexts Chemistry*. Retrieved from https://chem.libretexts.org/Bookshelves/Organic_Chemistry/Map%3A_Organic_Chemistry_(McMurry)/Chapter_25%3A_Biomolecules%3A_Carbohydrates/25.11_Cell-Surface_Carbohydrates_and_Influenza_Viruses
12. Gottlieb, S. (2019). Statement by FDA Commissioner Scott Gottlieb , M . D ., on preparations for the upcoming flu season and vaccinations, 1–5.
13. Horimoto, T. et al. (2005). Influenza: lessons from past pandemics, warnings from current incidents. *Nature Reviews Microbiology*, *3*(592).
14. Ito, T., Couceiro, J. N. S. S., Kelm, S., Baum, L. G., Krauss, S., Castrucci, M. R., … Kawaoka, Y. (1998). Molecular Basis for the Generation in Pigs of Influenza A Viruses with Pandemic Potential, *72*(9), 7367–7373.
15. Abdoli, M., Bahrami, F., Feizi, N., Kheiri, M. T., Mehrbod, P., … Saleh, M. (2016). Comparison between MDCK and MDCK-SIAT1 cell lines as preferred host for cell culture-based influenza vaccine production. *Biotechnology Letters*, *38*(6), 941–948. https://doi.org/10.1007/s10529-016-2069-4

16. Müller, L., Brighton, L. E., Carson, J. L., Fischer, W. A., & Jaspers, I. (2013). Culturing of Human Nasal Epithelial Cells at the Air Liquid Interface. *Journal of Visualized Experiments*, (80). doi:10.3791/50646
17. NEBioCalculator. (n.d.). New England Biolabs. Retrieved from https://nebiocalculator.neb.com/#!/ligation
18. Parrish, C. R., Murcia, P. R., & Holmes, C. (2015). Influenza Virus Reservoirs and Intermediate Hosts : Dogs , Horses , and New Possibilities for Influenza Virus Exposure of Humans, *89*(6), 2990–2994. https://doi.org/10.1128/JVI.03146-14
19. Qiagen. (2018). QIAquick Gel Purification Kit Protocol.
20. Qiagen. (2018). QIAprep Spin Miniprep Kit Protocol.
21. Qiagen. (2018). QIAquick PCR Purification Kit Protocol.
22. Qiagen. (2018). RNeasy Mini Kit Protocol.
23. Samji, T. (2009). Influenza A : Understanding the Viral Life Cycle, *82*, 153–159.
24. Schnirring, L. (2019). WHO reveals delayed pick for H3N2 flu vaccine strain, 2–4.
25. Seth J. Zosta, Kaela Parkhousea, Megan E. Guminaa, Kangchon Kimb, Sebastian Diaz Pereza, P. C. W., & John J. Treanord, Andrea J. Sante, Sarah Cobeyb, and S. E. H. (2017). Contemporary H3N2 influenza viruses have a glycosylation site that alters binding of antibodies elicited by egg-adapted vaccine strains. *PNAS*, *114*(47), 12578–12583. https://doi.org/10.1073/pnas.1712377114
26. Velthuis, A. J. W., & Fodor, E. (2016). Influenza virus RNA polymerase : *Nature Publishing Group*, *14*(8), 479–493. https://doi.org/10.1038/nrmicro.2016.87
27. Yao, T. (2017). cell culture media : History , characteristics , and current issues, (September 2016), 99–117. https://doi.org/10.1002/rmb2.12024
28. Zost, S. J., Parkhouse, K., Gumina, M. E., Kim, K., Diaz Perez, S., Wilson, P. C., … Hensley, S. E. (2017). Contemporary H3N2 influenza viruses have a glycosylation site that alters binding of antibodies elicited by egg-adapted vaccine strains. *Proceedings of the National Academy of Sciences*, *114*(47), 12578-12583. doi:10.1073/pnas.1712377114
29. Zymo Research. (2018). ZymoPURE II Plasmid Maxiprep Kit Protocol.
30. Centers for Disease Control and Prevention. (2019, March 26). Types of Influenza Viruses. Retrieved from https://www.cdc.gov/flu/about/viruses/types.htm
31. World Health Organization. (2018, November 13). Influenza (Avian and other zoonotic). Retrieved from https://www.who.int/news-room/fact-sheets/detail/influenza-(avian-and-other-zoonotic)
32. Centers for Disease Control and Prevention. (2017, September 27). How the Flu Virus Can Change: "Drift" and "Shift". Retrieved from https://www.cdc.gov/flu/about/viruses/change.htm
33. World Health Organization. (2018, February 22). Recommended composition of influenza virus vaccines for use in the 2018-2019 northern hemisphere influenza season. Retrieved from https://www.who.int/influenza/vaccines/virus/recommendations/2018_19_north/en/
34. New England Biolabs. (n.d.). 1 kb DNA Ladder. Retrieved from https://www.neb.com/products/n3232-1-kb-dna-ladder#Product%20Information

David M. Jacobs
May 20 1991
jacobsdavidmi@gmail.com
214-205-3872

Profile

Master of Science student studying molecular microbiology and immunology with an emphasis on virology. Laboratory researcher working with influenza strains.

Education

The University of Ottawa Faculty of Medicine
PhD in Biochemistry, Microbiology and Immunology
Anticipated start date in September 2019

Johns Hopkins Bloomberg School of Public Health
Science Masters in Molecular Microbiology and Immunology (in progress)
August 2017 – May 2019

- Cumulative GPA as of April 2019: 3.81
- Coursework focused on the immune system, different types of pathogens, as well as epidemiological tools to analyze and contain the spread of disease
- Thesis research on reassortment in human influenza A virus strains performed in Dr. Andrew Pekosz's laboratory

The University of Texas at Austin
Bachelor of Science in Biology with a Special Honors in Biology, May 2014

- Cumulative GPA: 3.68
- Special honors in recognition of completion of Dean's Scholars honors program emphasizing research
- Awarded UTeach Apprentice Teaching PBI (Project Based Instruction) Implementation Award for exceptional project design and implementation of "Serving Justice WITH SCIENCE!" unit in microbiology course for high school seniors in May 2015

Experience

Thesis Research, Pekosz Laboratory, Johns Hopkins Bloomberg School of Public Health
Baltimore, Maryland
October 2017 – Present

- Investigating currently circulating strains of influenza A H3N2 to determine genetic differences impacting observed virulence in 2017-2018 clinical isolates compared to 2016-2017 strains
- Techniques utilized included: cloning viral gene segments, viral growth curves on immortalized & primary human cell cultures, plaque assays, titering of viral samples, flow cytometry

Teacher, 9th Grade Biology, 12th Grade Aquatics and Environmental Sciences, Wakeland High School
Frisco, Texas
August 2015 – June 2017

- Coordinated with departmental teachers to design and implement lessons, prepare projects and assessments, teach students (~120 between all classes each year), be available for academic support and form positive relationships with students